Chapter 6
Dynamics in Semiconductor Lasers with Optical Injection

Since the semiconductor laser has unique features of high gain, low facet reflectivity, and amplitude-phase coupling through the α parameter, it is also sensitive to optical injection from a different laser. Locking and unlocking phenomena in optically injected semiconductor lasers have been extensively studied. Especially optical injection locking has been appreciated as a useful tool for controlling and stabilizing laser oscillations. The general application of optical injection is to control the laser and the locking condition is extensively investigated to distinguish the unlocking phenomena. However, little attention has been paid to the unlocking dynamics. Recent studies proved that rich varieties of dynamics, such as the four-wave mixing, period-doubling route to chaos, and non-locking beating, are involved in the unlocking region. In this chapter, we focus on the dynamic characteristics of locking and unlocking regimes in optically injected semiconductor lasers.

6.1 Optical Injection

6.1.1 Optical Injection Locking

Optical injection technique can be used in various applications, for example it is used to reduce intensity, frequency, and partition noises in semiconductor lasers (Furusawa 1996; Schunk and Petermann 1986; Genest et al. 1997), generating microwave signals (Chan and Liu 2004), or producing chaotic signals for secure communications (Liu et al. 2001). The technique is originally developed to lock the frequency and stabilize the oscillation of an optically injected laser. The injection locking system is very simple, as shown in Fig. 6.1. Injection locking is useful for stabilizing the injected laser; however, the lasers sometimes show instability and exhibit a rich variety of dynamics. For optical injection locking, we prepare two lasers with almost the same oscillation frequencies and the frequency detuning between them must usually be within several GHz. A light from a laser under a single

J. Ohtsubo, *Semiconductor Lasers*, Springer Series in Optical Sciences 111,
DOI: 10.1007/978-3-642-30147-6_6,

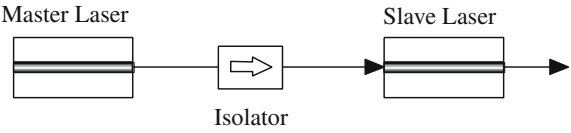

Fig. 6.1 Optical injection system in semiconductor lasers

mode oscillation (master laser) is fed into the active layer of the other laser (slave laser). Then, the two lasers synchronize with each other in the same optical frequency under the appropriate conditions of the frequency detuning and the injection strength. The remarkable characteristics of optical injection locking in semiconductor lasers originated from the fact that the α parameter (linewidth enhancement factor) has a nonzero definite value, which makes semiconductor lasers very different from other lasers. As a viewpoint of laser dynamics, an optical injection from a different laser means the introduction of an extra degree of freedom to the semiconductor laser. Therefore, various dynamics are observed by optical injection, including stable and unstable injection locking, instabilities and chaos, and four-wave mixing depending on the locking conditions (Mogensen et al. 1985; Sacher et al. 1992; Lee et al. 1993; Annovazzi-Lodi et al. 1994; Liu and Simpson 1994; Simpson et al. 1995, 1997; Kovanis et al. 1995; Erneux et al. 1996; De Jagher et al. 1996; Gavrielides et al. 1997; Eriksson and Lindberg 2001).

Optical injection technique is originally developed for the stabilization of the injected slave laser, so that, at first glance, it may be surprising that the laser is destabilized by the optical injection. However, as already mentioned, the perturbed laser is a candidate of a chaotic system. Figure 6.2a shows an example of bifurcation diagram of the slave laser for the change of the frequency detuning between the master and slave lasers at a fixed optical injection rate. We can see stable and unlocking oscillations, and various unstable oscillation states for the change of the frequency detuning. Figure 6.2b and c shows the time series and rf spectrum at the frequency detuning of $\Delta\nu = 1.0\,\mathrm{GHz}$. Similarly to chaotic oscillations for the case of optical feedback in the previous chapter, we can observe chaotic oscillations in optical injection systems. As we will see in the following, periodic and unstable oscillations are observed in adjacent to the stable injection locking state. Also, unlocking oscillations are distributed for large values of the frequency detuning. We will later present the instabilities and chaotic dynamics by optical injection and, here, we investigate the principle of optical injection locking in semiconductor lasers.

Again the tool for investigating the characteristics of optical injection locking is the linear stability analysis. We assume that the frequency detuning $\Delta\nu = \Delta\omega/2\pi$ between the master and slave lasers is small and the fraction of the photon number S_m (optical injection power $S_m = |E_m|^2 = A_m^2$) from a master laser is also small compared with the photon number S_s of a slave laser. As usual, the injection strength to the slave laser may or may not be small, but for the moment, we consider the case of a rather small optical injection. Here, we discuss the effects to understand the principle of optical injection locking. It is also noted that a laser may show instability and chaotic oscillations for a small injection fraction under certain injection conditions, as we will see in the following sections. We use a steady-state complex

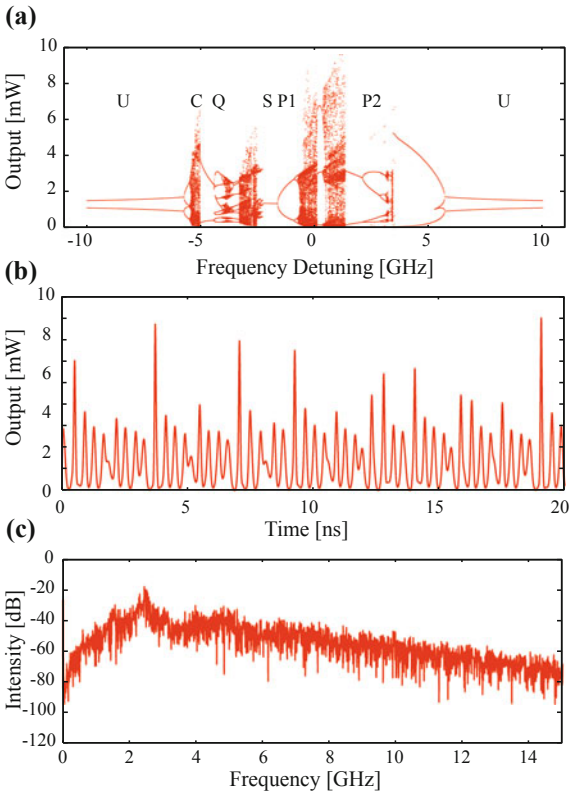

Fig. 6.2 **a** Bifurcation diagram for the frequency detuning at a fixed optical injection ration of $r_{\text{inj}} = 0.03$ (amplitude) and a bias injection current of $J = 1.3J_{\text{th}}$. **b** Example of the time series of chaotic states at the frequency detuning of $\Delta\nu = +1.0$ GHz. **c** The rf spectrum corresponding to **b**. Some examples of oscillation states in **a** are *S* stable injection locking state, *U* unlocking state, *P1* period-1 oscillation, *P2* period-2 oscillation, *Q* quasi-periodic oscillation, and *C* chaotic oscillation

field $E_m(t) = \sqrt{S_m}\exp\{-i\phi_m(t)\}$ for a master laser and assume the complex field $E_s(t) = \sqrt{S_s}\exp\{-i\phi_s(t)\}$ for a slave laser. The phases ϕ_m and ϕ_s are generally time-dependent functions, but the master laser is under steady-state operation and its phase is assumed to be constant as $\phi_m = 0$. Though the phase of the slave laser generally fluctuates with time, it is approximated as a small fluctuation and assumed to be a constant value in the following. Taking these assumptions into consideration, the rate equation for the slave field is written by

$$\frac{\mathrm{d}E_s(t)}{\mathrm{d}t} = \frac{1}{2}(1 - i\alpha)G_n\{n(t) - n_{\text{th}}\}E_s(t) + \frac{\kappa_{\text{inj}}}{\tau_{\text{in}}}E_m(t)\exp(-i\Delta\omega t) \tag{6.1}$$

where $\Delta\omega = 2\pi\Delta\nu = \omega_m - \omega_s$ is the detuning between the angular frequencies, ω_m and ω_s, for the master and slave lasers, respectively, κ_{inj} is the injection coefficient, and τ_{in} is the round trip time of light in the laser cavity as introduced before. κ_{inj} is related to the actual fraction of the external injection ratio r_{inj} (which is normalized to the average of the absolute value of the field $|E_s|$ as

$$\kappa_{\text{inj}} = \frac{r_{\text{inj}}}{r_0}\sqrt{\frac{1 - r_0^2}{\eta}} \tag{6.2}$$

where r_0 is the front facet reflectivity of the laser cavity and η is the refractive index of the laser medium, which are the same definitions as before. Even in the presence of optical injection, the carrier density equation accompanying to the field equation remains the same as (3.51).

Sometimes a different equation from (6.1) is used for investigating theoretically the dynamics of injection locking. In spite of the different expression, the same results as those derived from the rate equation in (6.1) are of course obtained. In this expression, using the angular frequency detuning parameter $\Delta\omega$, a new optical field $\tilde{E}_s(t)$ is defined as $E_s(t) = \tilde{E}_s(t)\exp(-i\Delta\omega t)$. Substituting the variable into (6.1) and eliminating the term $\exp(-i\Delta\omega t)$, we obtain the following new expression for the optical field:

$$\frac{\mathrm{d}\tilde{E}_s(t)}{\mathrm{d}t} = \frac{1}{2}(1-i\alpha)G_n\{n(t)-n_{\mathrm{th}}\}\tilde{E}_s(t) + \frac{\kappa_{\mathrm{inj}}}{\tau_{\mathrm{in}}}E_m(t) + i\Delta\omega\tilde{E}_s(t) \tag{6.3}$$

In the meanwhile, the carrier equation only includes the term for the absolute value of the field and has no modification. The field has an extra term of phase so that the dynamics are different from those of the original field itself. However, the resulting dynamics of the laser power and the carrier density remain the same as those derived from (6.1) and can be compared with experiments.

6.1.2 Injection Locking Condition

Optical injection locking is a coherent phenomenon, so that the discussion must be based on the complex field instead of the photon number. As the carrier density of the slave laser is affected by optical injection, we put the fluctuation of it as δn. We introduce a phase $\psi(t) = \phi_s(t) - \phi_m(t) - \Delta\omega$ and a small deviation between the photon numbers with and without the optical injection as $S_s - S_{0s}$ (S_{0s} is the photon number of the slave laser in the absence of the optical injection). By the use of the representation of $\psi(t)$ instead of $\phi_s(t) - \phi_m(t)$, we can define the rate equations as autonomous equations. Then, we obtain the solutions $S_s - S_{0s}$, ψ_s, and δn for the steady-state values (van Tartwijk and Agrawal 1998)

$$\frac{1}{2}G_n\delta n + \frac{1}{\tau_{\mathrm{in}}}\sqrt{\frac{S_{\mathrm{inj}}}{S_s}}\cos\psi_s = 0 \tag{6.4}$$

$$\Delta\omega = \frac{1}{2}\alpha G_n\delta n - \frac{1}{\tau_{\mathrm{in}}}\sqrt{\frac{S_{\mathrm{inj}}}{S_s}}\sin\psi_s \tag{6.5}$$

$$\delta n = -\left(\frac{1}{\tau_s} + G_n S_s\right)\delta n - \left(\frac{1}{\tau_{\mathrm{ph}}} + G_n\delta n\right)(S_s - S_{0s}) \tag{6.6}$$

where $S_{\rm inj} = \kappa_{\rm inj}^2 S_m$. In the above equation, replacing the fluctuation of the carrier density with $x = G_n \delta n$ and eliminating the variables ϕ_s and S_s, we obtain the characteristic equation as follows:

$$\begin{aligned} &-\frac{1}{4\tau_s}(1+\alpha^2)x^3 + \left\{\frac{1}{4}(1+\alpha^2)\omega_R^2 + \frac{1}{\tau_s}\right)x^2 \\ &-\left(\alpha\Delta\omega\omega_R^2 + \frac{\Delta\omega^2}{\tau_s} + \frac{1}{\tau_{\rm in}^2}G_n S_{\rm inj}\right)x + \omega_R^2\left(\Delta\omega^2 - \frac{1}{\tau_{\rm in}^2}\frac{S_{\rm inj}}{S_{0s}}\right) = 0 \end{aligned} \tag{6.7}$$

From the above equation, we obtain the solutions for the fluctuation of the carrier density. Eliminating δn in (6.4) and (6.5), we also obtain the relation between the phase ψ_s and the laser powers as

$$\psi_s = \sin^{-1}\left(-\frac{\tau_{\rm in}\Delta\omega}{\sqrt{1+\alpha^2}}\sqrt{\frac{S_s}{S_{\rm inj}}}\right) - \tan^{-1}\alpha \tag{6.8}$$

From this relation, we obtain the condition for the phase ψ_s as

$$-\frac{\pi}{2} - \tan^{-1}\alpha \le \psi_s \le \frac{\pi}{2} - \tan^{-1}\alpha \tag{6.9}$$

On the other hand, from the steady-state condition for the carrier density n_s under the existence of optical injection, one reads

$$\Delta n_s = n_s - n_{\rm th} = -\frac{2}{\tau_{\rm in}G_n}\sqrt{\frac{S_{\rm inj}}{S_s}}\cos\psi_s \tag{6.10}$$

Δn_s should be positive, so that the phase has the condition as $\psi_s \ge -\pi/2$. Therefore, the range of the phase for stable locking is totally given by Mogensen et al. (1985)

$$-\frac{\pi}{2} \le \psi_s \le \cot^{-1}\alpha \tag{6.11}$$

Finally, the range of the angular frequency for the stable injection locking condition is obtained as

$$-\frac{\sqrt{1+\alpha^2}}{\tau_{\rm in}}\sqrt{\frac{S_{\rm inj}}{S_s}} = \Delta\omega_L \le \Delta\omega \le \frac{1}{\tau_{\rm in}}\sqrt{\frac{S_{\rm inj}}{S_s}} \tag{6.12}$$

Successful optical injection locking occurs at a frequency satisfying the above equation for the injection fraction $S_{\rm inj}/S_s$. The α parameter encountered in the above equation plays an important role in optical injection locking.

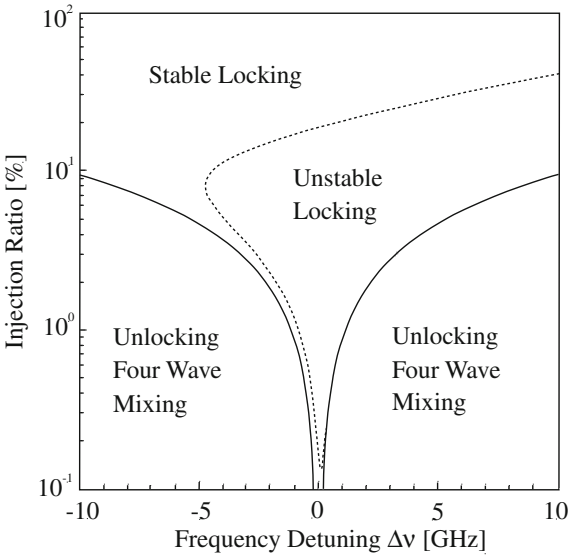

Fig. 6.3 Locking and unlocking regions in phase space of frequency detuning and injection field

Using the relation of (6.12), the fluctuation of the carrier density δn is given by

$$\delta n = \frac{2\alpha\Delta\omega \pm 2\sqrt{\Delta\omega_L^2 - \Delta\omega^2}}{G_n(1+\alpha^2)} \tag{6.13}$$

In the above equation, the plus and minus signs denote that the corresponding solution for (6.8) has a phase value of zero or π radian. There exist two solutions for the same photon number S_s. One is a stable solution and the other is unstable. In general, optical injection locking occurs at or close to the stable solution. Figure 6.3 shows the areas of optical injection locking in the phase space for the frequency detuning between the master and slave lasers and the injection ratio. The solid curves show the boundaries between optical injection locking and non-locking regions. In the non-locking region, we can expect various dynamics such as chaotic oscillations and four-wave mixing when the detuning is not so far from zero. Indeed, we can observe various dynamics when the frequency detuning and the injection ratio are small in these regions. Within the region of the optical injection locking, there are stable and unstable locking areas. The boundary of the unstable and stable injection locking areas is denoted by a dotted curve. In the unstable injection locking area, we can also observe chaotic bifurcations for certain parameter ranges. The asymmetric feature of stable injection locking again originated from the fact that the α parameter has a nonzero value in semiconductor lasers.

6.2 Stability and Instability in Optical Injection Systems

6.2.1 Rate Equations

Side modes are sometimes excited in the oscillation of a semiconductor laser subjected to optical injection even if it operates at a single mode under a solitary condition. Therefore, we must take into account the effect of side modes into the rate equations. The assumption of a single mode operation can be well applied to a DFB semiconductor laser. However, a single mode Fabry–Perot semiconductor laser, it is easily destabilized and oscillated at a multimode by the introduction of optical injection. Here, we first rewrite the rate equations of an optically injected semiconductor laser for a single-mode operation and, after that, we introduce the side mode effect. To investigate the dynamics of optically injected semiconductor lasers, we again introduce the equations of the field amplitudes for the master and slave lasers, $A_m(t)$ and $A_s(t)$, the phase $\psi(t)$, and the carrier density $n(t)$ as

$$\frac{\mathrm{d}A_s(t)}{\mathrm{d}t} = \frac{1}{2}G_n\{n(t) - n_{\mathrm{th}}\}A_s(t) + \frac{\kappa_{\mathrm{inj}}}{\tau_{\mathrm{in}}}A_m(t)\cos\psi(t) \tag{6.14}$$

$$\frac{\mathrm{d}\psi(t)}{\mathrm{d}t} = \frac{1}{2}\alpha G_n\{n(t) - n_{\mathrm{th}}\} - \frac{\kappa_{\mathrm{inj}}}{\tau_{\mathrm{in}}}\frac{A_m(t)}{A_s(t)}\sin\psi(t) - \Delta\omega \tag{6.15}$$

$$\frac{\mathrm{d}n(t)}{\mathrm{d}t} = \frac{J}{ed} - \frac{n(t)}{\tau_s} - G_n\{n(t) - n_0\}A_s^2(t) \tag{6.16}$$

$$\psi(t) = \phi(t) - \Delta\omega t \tag{6.17}$$

In the above equations, we do not consider the gain saturation terms, however, the gain saturation also plays an important role in multimode oscillations in semiconductor lasers with optical injection. For such a case, we can use the relation of (3.45) or (3.46) for the gain saturation effect.

When the side mode effects are important, the complex field for the main mode is rewritten as Ryan et al. (1994).

$$\begin{aligned}\frac{\mathrm{d}E_s(t)}{\mathrm{d}t} &= \frac{1}{2}(1 - i\alpha)G_n\{n(t) - n_{\mathrm{th}}\}E_s(t) \\ &\quad - \frac{1}{2}\left\{\varepsilon'|E_s(t)|^2 + \theta_c|E_{s'}(t)|^2\right\}E_s(t) + \frac{\kappa_{\mathrm{inj}}}{\tau_{\mathrm{in}}}E_m(t)\exp(-i\Delta\omega t)\end{aligned} \tag{6.18}$$

where $E_{s'}$ is the complex field of the side mode and θ_c is the cross-saturation coefficient for the gain. Here, we consider the excitation of one side mode and also take into account the self-saturation effect $\varepsilon' = \varepsilon_s(1 - i\alpha)G_n$. The rate equation for the complex field of the side mode is given by

$$\frac{\mathrm{d}E_{s'}(t)}{\mathrm{d}t} = \frac{1}{2}(1 - i\alpha)G_n\{n(t) - n_{\mathrm{th}}\}E_{s'}(t) - \frac{1}{2}\left\{\varepsilon'|E_{s'}(t)|^2 + \theta|E_s(t)|^2\right\}E_{s'}(t) - \mu_d E_{s'}(t) \tag{6.19}$$

where the final term is the gain defect of the secondary mode and μ_d is the coupling coefficient called gain defect.

Due to this gain defect, mode switching will be suppressed in this model and the laser is assumed to be always oscillated at the main mode as far as the coefficient has a significant value. Using these two modes, the carrier density equation is written by

$$\frac{\mathrm{d}n(t)}{\mathrm{d}t} = \frac{J}{ed} - \frac{n(t)}{\tau_s} - G_n\{n(t) - n_0\}\left\{|E_s(t)|^2 + |E_{s'}(t)|^2\right\} \tag{6.20}$$

In actual fact, many side modes may be excited in the laser oscillations due to optical injection. However, it is proved that the model introduced here well explains mode excitations for real oscillations in a Fabry–Perot semiconductor laser subjected to optical injection.

The laser gain is usually linearized for the carrier density. However, in a strict sense, it is also a function of the photon number and the gain term $g' = (1 - i\alpha)G_n\{n(t) - n_{\mathrm{th}}\}$ is replaced by

$$g' = (1 - i\alpha)G_n\{n(t) - n_{\mathrm{th}}\} + (1 - i\alpha')G_P\left\{|E(t)|^2 - |E_0|^2\right\} \tag{6.21}$$

where G_P is the expansion coefficient for the photon number $S = |E|^2$, α' is the coefficient for the saturation of the output power, and E_0 is the steady-state field amplitude. For the model of a two-level atom in laser oscillations, we can approximate the coefficient α' equal to α, while it reduces to zero under the resonance condition (Simpson et al. 2001). Stability and instability of semiconductor lasers for optical injection are strongly dependent on the linewidth enhancement factor α and also on the coefficient α' of the saturation. It is proved in the following that this nonlinear coefficient α' is related to the suppression of the laser instabilities. Namely, the laser is stabilized for a larger value of this factor, while it shows instabilities for a small value of it. The damping term μ_d introduced in the side mode equation in (6.19) also plays an important role in the dynamics as discussed in the following.

In semiconductor laser systems of optical injection, optical feedback, and optoelectronic feedback, we can observe multi-stability and coexistence states of chaotic oscillations in the dynamics. At coexistence states, the respective chaotic attractor is completely different from others even for a particular set of the parameter values. Which state we can observe is strongly dependent on the initial conditions of the systems. Coexistence states of attractors are not only simulated by numerical calculations, but also experimentally observed. Some such examples in optical injection systems will be discussed in Sect. 6.2.4.

6.2.2 Chaotic Bifurcations by Optical Injection

The important parameters in the dynamics of optically injected semiconductor lasers are the frequency detuning between the master and slave lasers and the injection strength from the master to the slave. Figure 6.4 shows the experimental results of the dynamic characteristics in a semiconductor laser subjected to optical injection (Simpson 2003). The figure shows the plots of optical frequencies observed by a Fabry–Perot spectrometer (left column) and rf power spectra obtained by a spectrum analyzer (right column). Chaotic bifurcations are well demonstrated by the plots. We can assume a single mode operation for the semiconductor laser even in the presence of optical injection, since the laser used is a DFB laser. As is easily recognized from the stability map in Fig. 6.3, the slave laser operates outside of the stable locking region for a small optical injection. When the injection fraction exceeds a certain threshold, the laser is injection-locked by the master laser and operates stably. It is noted that the injection strength defined in the figure is counted outside of the laser and not exactly equal to the intensity injected into the active layer.

In Fig. 6.4a, for a small level of the injection rate of 0.14, the slave laser shows four-wave and multi-wave mixing associated with the unlocked slave laser frequency and has a side peak in the spectrum due to regenerative amplification. The effect of multi-wave mixing becomes distinct in the laser output power at the injection rate of 0.23 in Fig. 6.4b. At the same time, the component corresponding to the relaxation oscillation becomes non-vanishing and the oscillation close to the relaxation oscillation frequency of 4.7 GHz is excited. Also, the spectrum is much broadened. The multi-wave mixing effect is recognized as the phase-modulation like Adler-type frequency pulling toward locking (Simpson 2003). However, the frequency pulling here is somewhat different from the ordinary effect and it is an unstable phenomenon accompanying the relaxation resonance. Frequency-pulled multi-wave mixing components disappear at the injection rate of 0.41 and the multi-wave mixing features are pulled to the injection frequency as shown in Fig. 6.4c. As a result, a sharp and enhanced component of the relaxation oscillation is observed. Therefore, the laser shows a stable oscillation under the condition. Incommensurate frequency is encountered in the dynamics at the injection rate of 0.52 in Fig. 6.4d and the floor of the spectrum becomes broadened. This is a typical feature of the onset of quasi-periodic bifurcation and chaos. The floor of the spectrum further becomes broadened at the injection rate of 0.77 in Fig. 6.4e and several spectral peaks appear except for the relaxation oscillation component. Within the main peak, we can see two visible peaks. This indicates that the laser corresponds to period-3 oscillation. The oscillation mode within the relaxation oscillation frequency reduces as a single peak at the injection rate of 1.02 and the laser shows period-2 oscillation as shown in Fig. 6.4f. When the injection fraction is large enough at the injection rate of 1.30 in Fig. 6.4g, the laser oscillates at period-1 oscillation with the main frequency corresponding to the relaxation oscillation. The higher harmonics of the period-1 oscillation is also visible. Finally in Fig. 6.4h, at a strong injection rate of 3.01, the laser is completely locked to a certain frequency and shows period-1 oscillation. The locked frequency

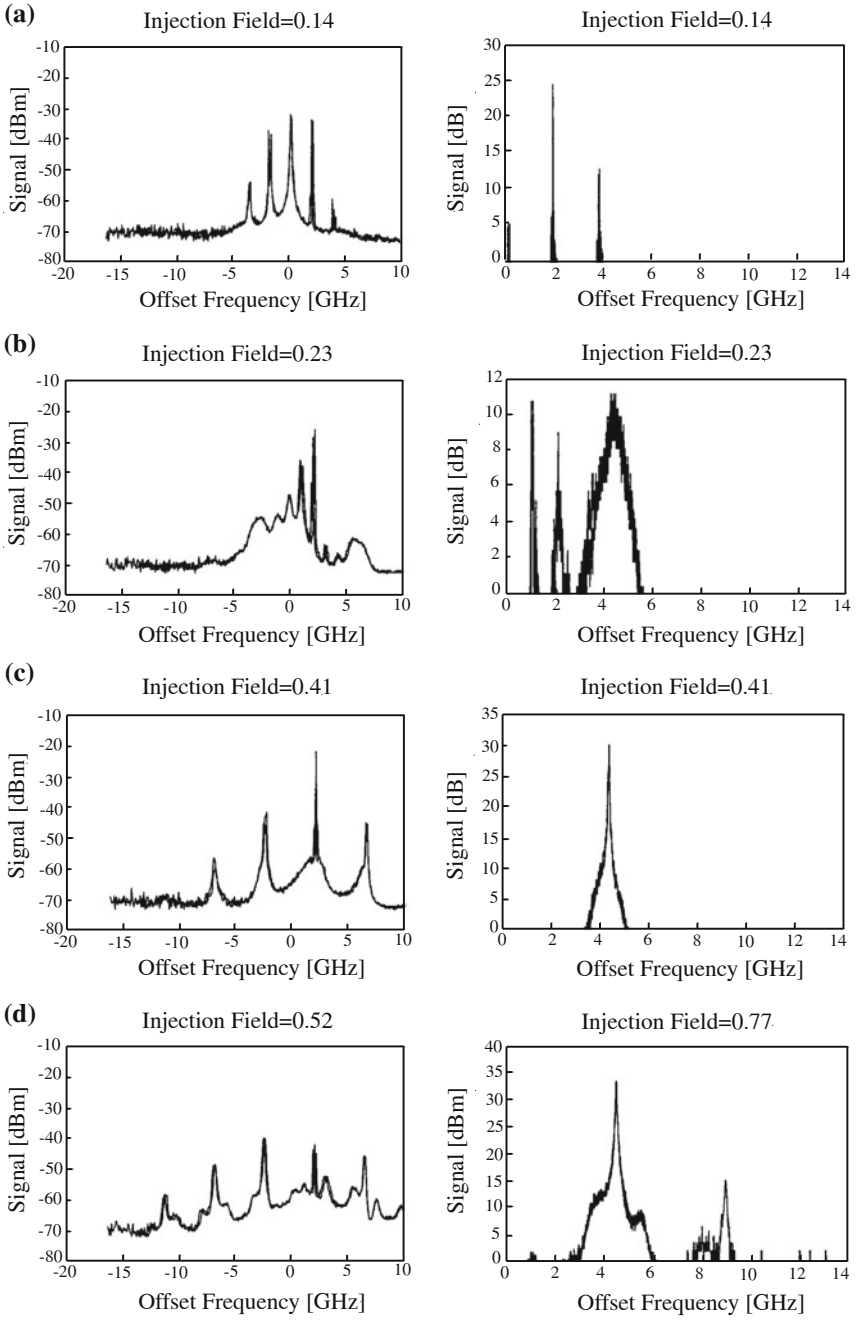

Fig. 6.4 Experimentally observed optical frequencies and rf power spectra corresponding to chaotic bifurcation in semiconductor lasers under optical injection. On the *left* are optical spectra and the *right* are rf spectra. The laser is a single mode DFB laser at a wavelength of 1.557 μm and a bias injection current of $J = 2.0J_{\text{th}}$

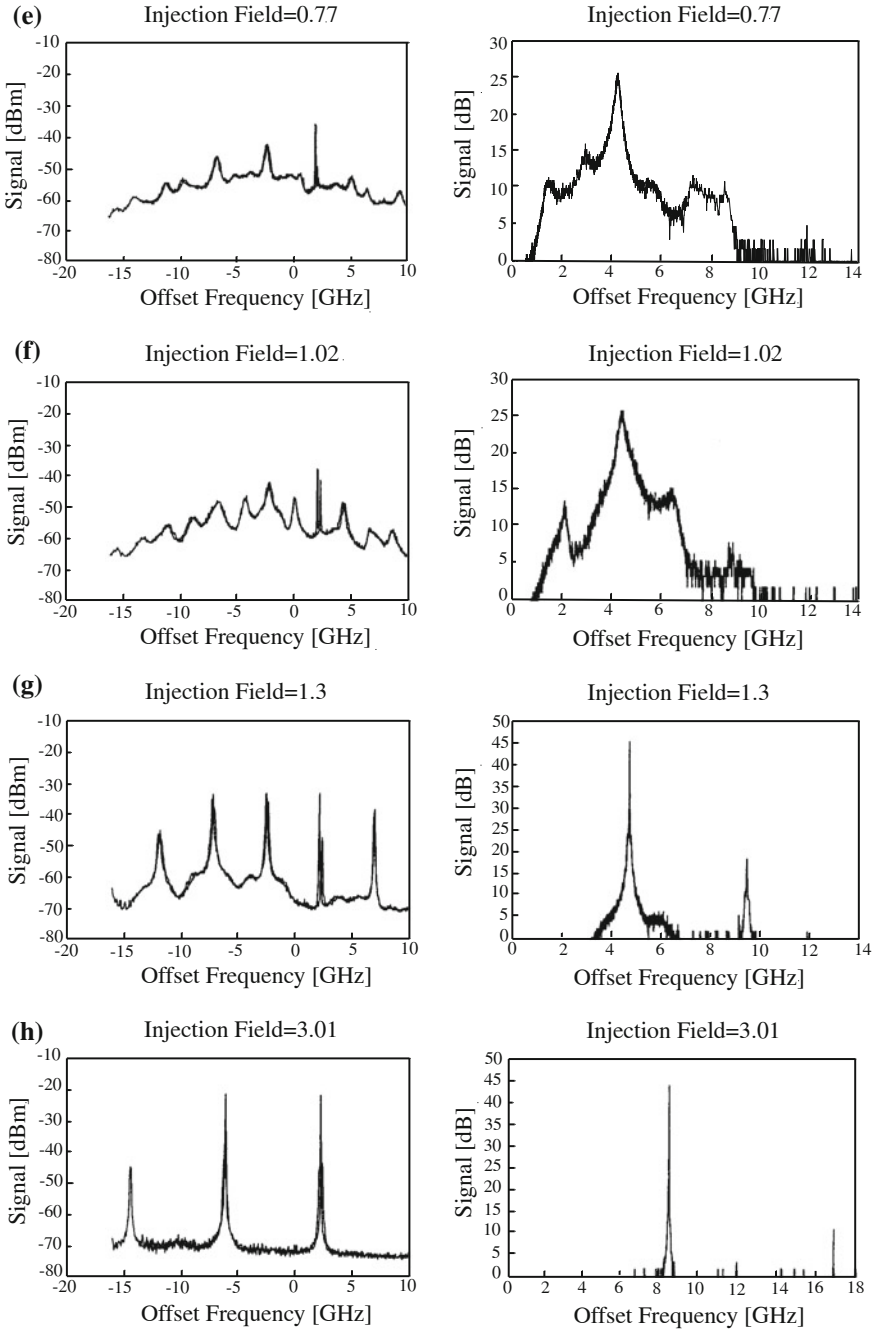

Fig. 6.4 (continued) The relaxation oscillation frequency at solitary oscillation is 4.7 GHz. The injection rate (intensity) is changed as **a** 0.14, **b** 0.23, **c** 0.41, **d** 0.52, **e** 0.77, **f** 1.02, **g** 1.30, and **h** 3.01, respectively, at the fixed frequency detuning of +2 GHz [after Simpson (2003); © 2003 Elsevier]

is different from the relaxation oscillation frequency at the solitary oscillation. This phenomenon is related to the enhancement of the cutoff frequency for the modulation bandwidth of the laser as discussed in the following. In this example, the chaotic evolution is observed for a fixed frequency detuning (+2 GHz). The dynamics are not always the same as those for other conditions of the detuning, but they exhibit typical chaotic routes when the absolute value of the frequency detuning is within several GHz.

In accordance with stable and unstable oscillations in optically injected semiconductor lasers, chaotic bifurcations are numerically calculated taking into consideration the effects of side mode excitation. Figure 6.5 shows chaotic bifurcations for a change of the injection ratio at a fixed frequency detuning of +2 GHz (Simpson 2003). In Fig. 6.5a, the laser is assumed to be oscillated at a single mode, since it includes the effect of a larger defect with $\mu_d = 0.1$. The laser once evolves from periodic to chaotic oscillations and, then, takes an inverse route of chaotic bifurcations for the increase of the injection ratio. Finally, it reduces to the period-1 state. The behaviors are quite similar to the chaotic route for a single mode laser discussed in Fig. 6.4 On the other hand, the instability of the laser is suppressed because of the leakage of the power from the main mode to the side mode when the effect of the defect is as small as $\mu_d = 0.001$ in Fig. 6.5b. Under this condition, the laser shows no typical chaotic bifurcations. Figure 6.5c shows the plot of the relative circulating power level in the main mode for single and multimode operations. The power of the main mode is transferred to the side mode and the instability of the laser oscillation is greatly suppressed, when there is a side mode and the injection strength is small. However, the side mode is never excited for a larger value of the defect and the assumption of a single mode oscillation is well established.

6.2.3 Chaos Map in the Phase Space of Frequency Detuning and Injection

We discuss chaos maps in the phase diagram of the frequency detuning and the injection ratio. Stable injection locking is achieved in a region for a certain combination of the frequency detuning and the injection ratio; however, various unstable and chaotic dynamics are observed in unstable locking and unlocking regions. Figure 6.6 shows the chaotic map obtained experimentally from the behaviors of the optical spectra in Fig. 6.5 (Simpson 2003). The laser is operated at a single mode even in the presence of optical injection and the side mode is suppressed in this laser. It is noted that the vertical axis and the horizontal axis are replaced compared with the plot in Fig. 6.3. The diamond-filled symbol shows in the negative frequency detuning is the boundary between unstable and stable operations. This corresponds to the saddle node boundary between stable locked and unlocked operations. Open diamonds show the unlocking-locking transition in a region of bistability and torus bifurcation. The square mark close to zero detuning is the Hopf bifurcation boundary between stable locked and limit cycle dynamics. The triangle is the boundaries for regions of

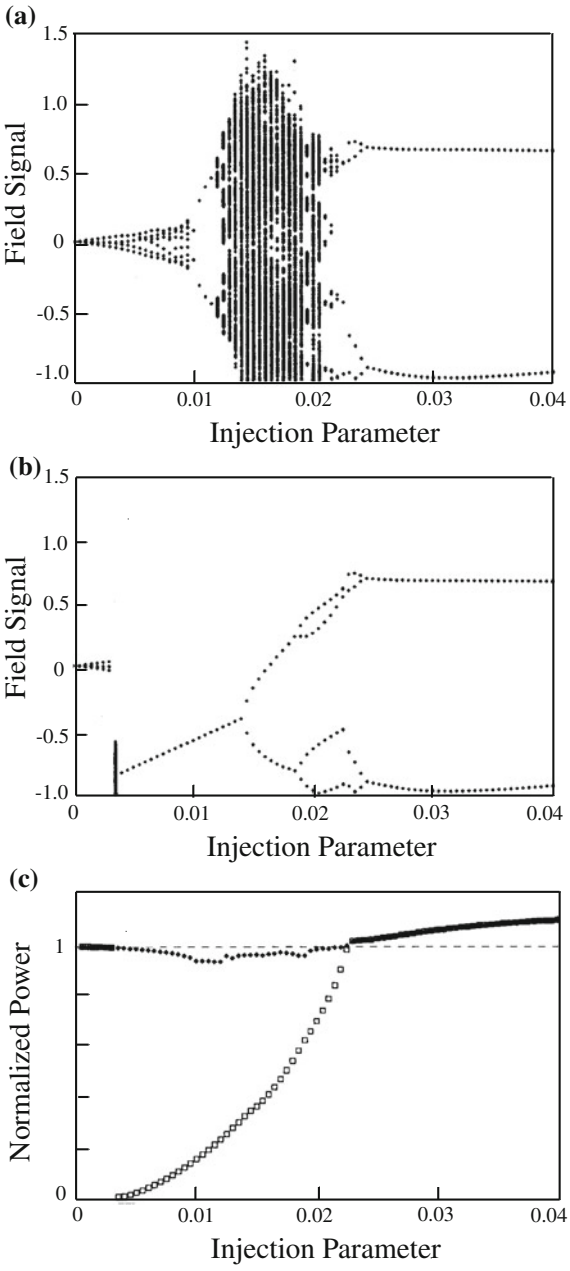

Fig. 6.5 Bifurcation diagram as a function of the injection ratio at a frequency detuning of +2 GHz. **a** Bifurcation diagram for large gain defect of $\mu_d = 0.1$. The laser oscillates at a single mode. **b** Bifurcation diagram for a small gain defect of $\mu_d = 0.001$. Significant power leaks into the side mode. **c** Relative circulating power. The symbol of *diamonds* is for the single mode oscillation, while *open squares* denote the case of multimode oscillations [after Simpson (2003); © 2003 Elsevier]

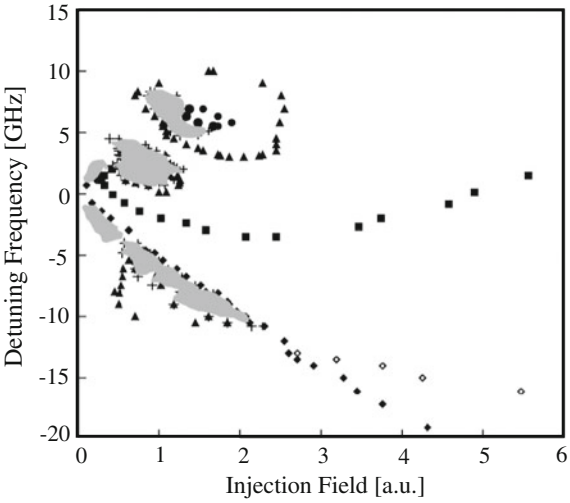

Fig. 6.6 Experimentally obtained chaotic map from measured optical spectra of a single mode DFB laser under optical injection. The meaning of each symbol is referred to the text [after Simpson (2003); © 2003 Elsevier]

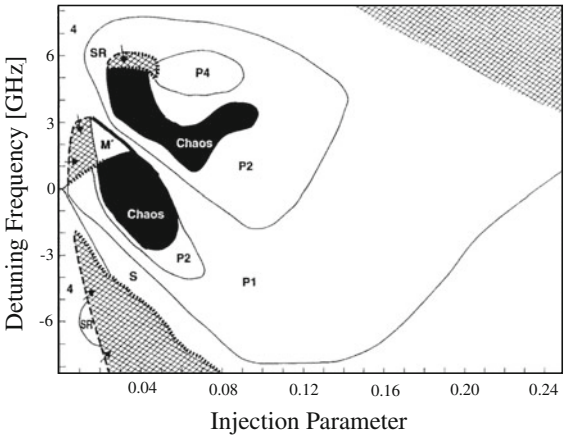

Fig. 6.7 Experimentally obtained chaotic map from measured optical spectra in a Fabry–Perot laser operating at 827.6 nm. A side mode is excited by optical injection. The bias injection current is $J = 1.67 J_{\text{th}}$. The detail of the map is discussed in the text [after Hwang and Liu (2000); © 2000 Elsevier]

period-2 dynamics. These period-2 regions include complex dynamics and they are shown by the shaded lines and crosses in the figure. Bounded by the circles is a region of period-4 operation. At injection levels below the saddle node bifurcation line and at low offset frequencies, multi-wave mixing and Adler-type frequency pulling to locking are observed in the lightly shaded regions.

Figure 6.7 shows the experimental result for the map in a semiconductor laser with side mode excitation by optical injection (Hwang and Liu 2000). The laser used is a conventional Fabry–Perot type edge-emitting laser with a quantum well structure. The back facet of the laser is coated for high reflection and the front output facet is coated for a reflection of a few percent. At the free running state of the laser oscillation, the side mode is suppressed as low as less than 0.5 %. The symbols in

the figure are 4: a perturbation spectrum with weak regenerative amplification and four-wave mixing sidebands, S: stable injection locking, P1: limit cycle oscillation, P2: period doubling, P4: period quadrupling, chaos: deterministic chaos, M: multi-wave mixing with most output on another longitudinal mode, SR: sub-harmonic resonance, hatched regions: principal output on another longitudinal mode, thin curves: smooth transition between dynamic regions, thick dotted curves: abrupt mode hop transitions with minor hysteresis, thick broken curves with an arrow: one-way mode hops out of mode, and thick full curves: abrupt transition to/from a region of chaos or multi-wave mixing where there is significant power in another longitudinal mode, from/to a region with power primarily in the principal mode.

For a small injection, the optical injection acts as a perturbation generating weak sidebands at the offset frequency, regenerative amplification, and equally and oppositely shifted four-wave mixing. With increasing both of the frequency detuning and the injection ratio, various instabilities appear in the laser output power. The tendency of periodic bifurcations and chaotic islands in the unstable region is the same as that for a DFB laser. However, distinct chaotic bifurcation is not observable for a Fabry–Perot laser in the region of negative frequency detuning along the stable boundary, while it was observed for a DFB laser (see Fig. 6.6). There is an abrupt mode hop near the locking–unlocking boundary at negative detuning which has a small hysteresis. Analytical studies of the locking–unlocking boundary at negative detuning have shown that there is a region of bistability associated with the locking–unlocking transition (Li, 1994a,b). The bistability results from competing attractors representing locked and unlocked solutions for the coupled equations (Lenstra et al. 1993). The carrier density is larger than that for the steady-state n_s under the unlocked solution, while it stays a smaller value for the locked solution. The gain of the side mode increases with the increase of the carrier density and the refractive index of the active layer accordingly changes. The change induces the transfer of the optical energy from the main mode to side modes. Then, the gain of the main mode is reduced and this sometimes results in frequent mode hop. However, the chaotic dynamics disappears in the output power. On the contrary, instabilities still remain in the dynamics of a single mode laser without the excitation of the side mode as shown in Fig. 6.6.

Considering the gain defect and using the Eqs. (6.18)–(6.20), stable and unstable maps in the phase space of the frequency detuning and the injection ratio like in Figs. 6.6 and 6.7 can be calculated (Simpson 2003). The results are quite consistent with the experimental results. Namely, the suppression of chaotic dynamics for the excitation of the side mode is well reproduced. Hwang and Liu (2000) numerically calculated maps of stable and unstable regions in the phase space of the frequency detuning and the injection ratio by changing the parameters in the rate equations. They studied the dependence of the parameters for the cavity decay rate $\gamma_c = 1/\tau_{\mathrm{ph}}$, the carrier relaxation rate $\gamma_s = 1/\tau_s$, the differential relaxation rate γ_n, and the nonlinear carrier relaxation rate γ_π. For the change of those parameters, they obtained the following results. (1) The carrier decay rate γ_s affects little change, since the carrier relaxation is usually induced by spontaneous emission of light and it is a small perturbation for the field strength. (2) The laser is stabilized for a small value

of the differential relaxation rate γ_n, since the fast carrier diffusion reduces unstable regions. (3) When the nonlinear carrier relaxation rate γ_π increases, the unstable region shrinks and the laser is stabilized. The increase of the nonlinear carrier relaxation rate γ_π results in the change of the carrier density in the active layer and the fluctuation of the optical phase is suppressed. This results in the suppression of frequency fluctuations. Therefore, the laser is stabilized. (4) For a larger value of the α parameter, instability of laser oscillation is enhanced. (5) Stability and instability of semiconductor lasers subjected to optical injection are also dependent on the bias injection current. With increasing the bias injection current, the stable region in the map expands. When a laser is operated at a higher injection current level, the coherent optical power stored in the cavity is higher, thus allowing the laser to be more resistant to the perturbation of the externally injected optical field. This is why stronger externally optical perturbation is required to observe instabilities and chaos in the system at a higher injection current level.

6.2.4 Coexistence of Chaotic Attractors in Optically Injected Semiconductor Lasers

A nonlinear system has the nature of multi-stability under a certain condition of the parameters. Namely, the system may have coexistent states of different chaotic attractors for the same parameter set. Which attractor the system converges to strongly depends on the initial conditions. Indeed, coexistence of chaotic orbits has been observed in various systems of semiconductor lasers (Masoller and Abraham 1998; Heil et al.1998, 1999; Sukow et al. 1999; Viktorov and Mandel 2000). In optically injected semiconductor lasers, multi-stability and coexistence of chaotic attractors have also been studied (Wieczorek et al. 2000, 2001a, 2001b, 2001c, 2002). Here, we present such examples. Under a certain experimental configuration, we always observe a particular chaotic attractor, since the process of obtaining chaotic oscillation is generally the same. Therefore, we usually observe a chaotic oscillation for one of the chaotic attractors in a fixed experimental condition even if multi-stabilities are involved in the system. However, if the separation between the two coexisting attractors in the high-dimensional phase space is not so far away, switching from one attractor to the other may occur due to, for example, noises involved in the system. Indeed, transition of the state from one chaotic oscillation to another has been experimentally observed (Heil et al. 1998, 1999).

Using the bifurcation theory, it is easy to know whether a nonlinear system has coexisting attractors under the operating condition when the system exhibits bistability or multi-stability. However, the characteristics of the coexisting attractors cannot be obtained using the bifurcation analysis. With the simulation method, the existence of the bistability or multi-stability is found by numerically simulating the system with different initial conditions under the same operating conditions. Figure 6.8 shows the numerical result for the map of coexistence states in semiconductor lasers subjected

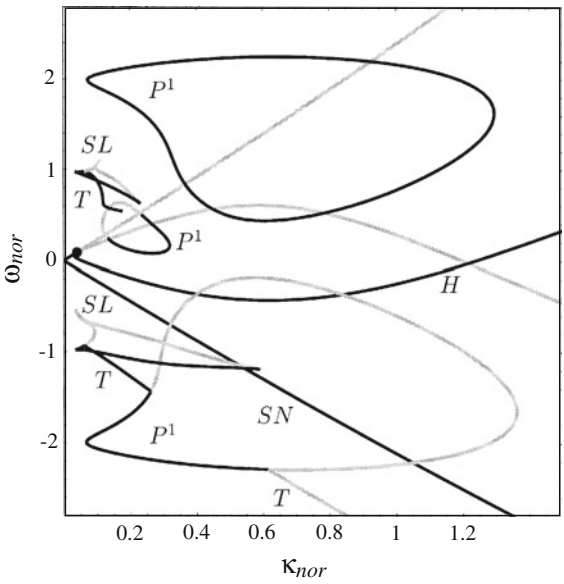

Fig. 6.8 Bifurcation diagram showing coexistence states in a phase space of normalized frequency detuning and injection ratio. The *vertical axis* is the normalized frequency of $\omega_{\text{nor}} = \Delta\omega/\omega_R$, and the *horizontal axis* of the injection ratio is also normalized as $\kappa_{\text{nor}} = \kappa_{\text{inj}} A_m/\omega_R \tau_{\text{in}} A_{0s}$. P^1 period-doubling bifurcations, *SL* saddle-nodes of limit cycles, *T* torus, *H* Hopf bifurcation, and *SN* saddle-node bifurcation [after Wieczorek et al. (2000); © 2000 Elsevier]

to optical injection (Wieczorek et al. 2000). The plot is a similar one in the phase space as shown in Figs. 6.6 and 6.7, but normalized axes are used. Each point in this plane corresponds to a particular phase portrait, which contains more than one attractor. Black parts of bifurcation curves correspond to supercritical bifurcations in which attractors bifurcate and gray parts correspond to subcritical bifurcations of repelling objects. Subcritical bifurcations are less important from an experimental point of view, but we trace them out as they may produce stable objects for instance in a subcritical torus bifurcation or change to supercritical.

In Fig. 6.8, the region inside the straight line from zero detuning to negative detuning is the stable injection locking area. A detailed explanation of the map is found in the reference (Wieczorek et al. 2000). We here focus on the points that weigh with actual observations. In the stable region, there exist areas for the saddle-node bifurcation (SN) and the Hopf bifurcation (H). When the black part of SN is crossed, one of the bifurcating stationary points is an attractor. It physically corresponds to the laser operating at constant power and at the frequency of the injected light, meaning that the laser locks to the input signal. On the other hand, along the gray part of the curve SN, a repellor and a saddle point bifurcate. Along the black part of H, an attracting periodic orbit is born from the attracting stationary point and this corresponds physically to the undamping of the relaxation oscillation. Physically, the appearance of a new orbit means that some resonance in the laser gets excited, often because the operational parameters $\kappa_{\text{nor}} = \kappa_{\text{inj}} A_m/\omega_R \tau_{\text{in}} A_{0s}$ and $\omega_{\text{nor}} = \Delta\omega/\omega_R$ drive the laser close to the relaxation frequency or its multiples. In Fig. 6.8, the two saddle nodes of the limit cycle bifurcation curves starting with a cusp at $\omega_{\text{nor}} \approx \pm 1$

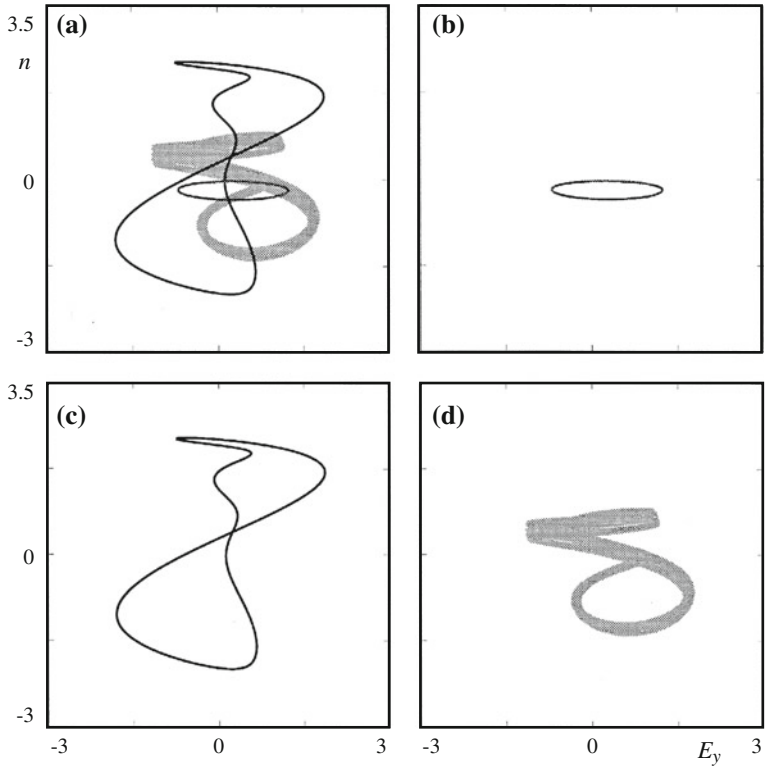

Fig. 6.9 Coexistence state of attractors at $\kappa_{\text{nor}} = 0.29$ and $\omega_{\text{nor}} = -1.37$. **a** Simultaneous plot of three attractors, **b** running phase solution, **c** large periodic orbit, and **d** quasi-periodic motion on a torus [after Wieczorek et al. (2000); © 2000 Elsevier]

represent a resonance between the relaxation oscillation frequency of the laser and the detuning of the injected light from the free running laser frequency.

Starting from different initial conditions, the nonlinear system may have different attractors in the phase space, even if the parameters have the same values as shown in the previous figure. Figure 6.9 shows examples of attractors in multistability states in the phase space of the imaginary part of the field, E_y (where the complex field E is given by $E = E_x + iE_y$), and the carrier density n (Wieczorek et al. 2000). The plots are the same conditions as those in Fig. 6.8. Figure 6.9a shows the plot of three attractors. Figure 6.9b and c is periodic states of period-1 with small amplitude and large periodic orbit, respectively. Figure 6.9d corresponds to a quasi-periodic oscillation on a torus. As has already been discussed, which of the attractors the system settles down to depends on the initial conditions. Furthermore, when a parameter is swept gradually through a region of multi-stability, then one will find hysteresis loops with sudden jumps from one attractor to another at different values of the parameter, depending on the direction of the sweep.

6.3 Enhancement of Modulation Bandwidth and Generation of High Frequency Chaotic Oscillation by Strong Optical Injection

6.3.1 Enhancement of Modulation Bandwidth by Strong Optical Injection

The modulation bandwidth of a semiconductor laser at free running state is limited by the relaxation oscillation frequency. However, when a semiconductor laser is strongly injected under stable conditions, the modulation bandwidth of the slave laser is greatly enhanced. At the same time, the suppression of laser noises is achieved, but the strong modulation gives rise to frequency chirping in the laser oscillation. The effects of noises and frequency chirping under optical injection are critical for the laser operation (Piazzolia et al. 1986; Yabre 1996). In a locking–unlocking bistable state, a large modulation current can unlock the laser. In a state near or beyond the Hopf bifurcation boundary, the dynamic instability of the laser can lead to high broadband noise and large frequency chirping. Also, the enhancement of the modulation bandwidth of semiconductor lasers subjected to strong injection has been demonstrated (Simpson et al. 1995, 1996; Simpson and Liu 1997; Chen et al. 2000; Wang et al. 1996, 2008). For weak optical injection and optical feedback, the modulation bandwidth is increased due to the increase of the photon number within the internal cavity, since the relaxation oscillation frequency is proportional to the square root of the photon number (see (3.71)). The amount of the shift of the cutoff frequency is up to ten percent at most. However, the cutoff frequency of the laser under strong optical injection is greatly enhanced up to several times the relaxation oscillation frequency of the free running laser. Therefore, a different explanation for the origin of the enhanced modulation bandwidth may be required to understand the phenomenon. The bandwidth-enhanced semiconductor laser is very useful as a broadband light source for optical communications.

Figure 6.10 is an example of experimental results of the enhancement of the modulation bandwidth. For a modulation of a small sinusoidal wave of 12 GHz to the bias injection current, the modulated laser output attenuated and is only −27.49 dBm without optical injection as shown in Fig. 6.10a, since the modulation is far away from the relaxation oscillation frequency (about 3 GHz). On the other hand, the modulation efficiency is increased up to 10 dBm by a strong optical injection (Fig. 6.10b). As will be discussed in Chap. 13, chaotic carrier frequency is the measure of the maximum data transmission rate in secure optical communications based on chaos synchronization in semiconductor laser systems. The chaotic carrier frequency is also increased by a strong optical injection and a large capacity of the channels for the communication is expected.

The enhancement of the modulation bandwidth in a semiconductor laser under strong optical injection is numerically studied based on the rate equations. Wang et al. (1996) investigated the modulation response for a small signal to the bias injec-

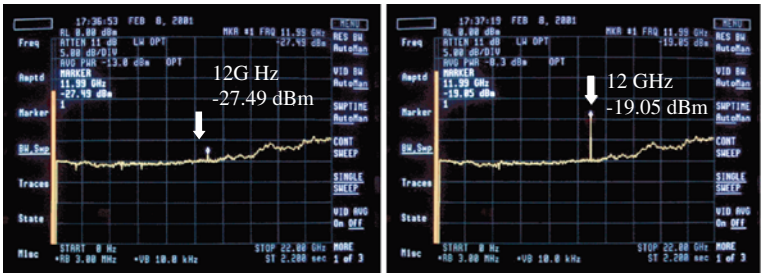

Fig. 6.10 Experimental result of the modulation bandwidth of a strongly optical injection-locked semiconductor laser. The laser is modulated by a small sinusoidal signal at 12 GHz. The modulation efficiency without optical injection is −27.49 dBm. The efficiency with optical injection is −19.05 dBm. The relaxation oscillation frequency of the DFB laser used is 3 GHz at free running state

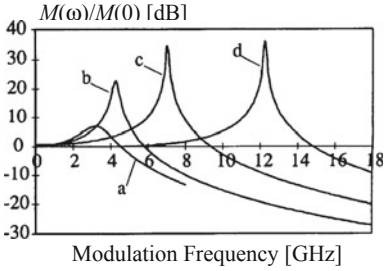

Fig. 6.11 Normalized modulation response of a semiconductor laser at $J = 2.4J_{\text{th}}$. **a** free running laser, **b** $S_{\text{inj}}/S_s = 0.011$, **c** $S_{\text{inj}}/S_s = 0.092$, **d** $S_{\text{inj}}/S_s = 0.44$. S_{inj} and S_s are the photon numbers injected from the master laser and the steady-state value of the free running slave laser [after Wang et al. (1996); © 1996 IEEE]

tion current using a linear stability analysis. Figure 6.11 is the result. The frequency detuning between the master and slave lasers is assumed to be zero in this case. The cutoff frequency read from the resonance frequency is 12.6 GHz for the injection ratio of $S_{\text{inj}}/S_s = 0.44$ (curve d), while the relaxation oscillation frequency is 3.4 GHz at the free running state (curve a). In addition, the response is almost flat well below the cutoff frequency and the modulation bandwidth is enhanced up to four times compared with that of the free running state. As has already been discussed, the relaxation oscillation frequency is proportional to the square root of the photon number and the photon number is a function of the bias injection current. To obtain the equivalent modulation bandwidth of 12 GHz for the free running laser, we would require the bias injection current to be seven times larger than that of the free running state, which corresponds to almost 13 times the threshold injection current and might damage the laser. Thus, the method of strong optical injection is effective for greatly enhancing the modulation bandwidth in semiconductor lasers. Wang et al. (1996)

conducted a linear stability analysis for the cutoff frequency under strong optical injection and obtained the approximate solution as

$$\nu_{\text{enhanced}} = \frac{1}{2\sqrt{3}\pi}\left[K_e - \left(\frac{K_a}{S_s}\right)^2 + \left\{\left(\frac{K_a}{S_s}\right)^2 - 4K_e\left(\frac{K_a}{S_s}\right)^2 + K_e^2 - 6K_aK_b\alpha G_n^2(n_s - n_0)\right\}^{1/2}\right]^{1/2} \tag{6.22}$$

where the parameters in the above equation are given by

$$K_e = \frac{1}{\tau_{\text{in}}^2}\frac{S_{\text{inj}}}{S_s} \tag{6.23}$$

$$K_a = \frac{2}{\tau_{\text{in}}}\sqrt{S_{\text{inj}}S_s}\cos(\phi_s - \phi_m) = -\left\{G_n(n_s - n_0)(1 - \varepsilon_s S_s) - \frac{1}{\tau_{\text{ph}}}\right\}S_s - R_{sp} \tag{6.24}$$

$$K_b = \frac{1}{\tau_{\text{in}}}\sqrt{\frac{S_{\text{inj}}}{S_s}}\sin(\phi_s - \phi_m) = \frac{1}{2}\alpha G_n(n_s - n_0) - \Delta\omega \tag{6.25}$$

As will be shown later, the cutoff frequency is linearly proportional to the injection power. Therefore, the origin of the enhancement of the modulation bandwidth does not simply come from the increase of the photon number in the active layer. It is explained by the interference between the optical frequency of the original laser oscillation and the shifted frequency due to the strong optical injection.

The enhancement of the modulation bandwidth is also strongly dependent on frequency detuning between the master and slave lasers. Figure 6.12 shows the dependence of the modulation response in the presence of frequency detuning between the master and slave lasers (Chen et al. 2000). The conditions of the numerical simulations are as follows; the laser is assumed to be an index-guided GaAs/AlGaAs quantum-well laser and is biased at $\hat{J} = 0.67$ (corresponding to $J = 1.67J_{\text{th}}$), where $\hat{J}$ is the scaled injection current defined by $\hat{J} = (J/ed - n_s/\tau_s)/(n_s/\tau_s)$. The injection parameter defined by $\kappa'_{\text{nor}} = (\kappa_{\text{inj}}\tau_{\text{ph}}A_m)/(\tau_{\text{in}}A_s)$ is fixed at a moderate level of $\kappa'_{\text{nor}} = 0.2$, while different values of frequency detuning representing different locking conditions are chosen. At $\kappa'_{\text{nor}} = 0.2$, the stable locking region is bounded by $\Delta\nu = 1$ GHz and $\Delta\nu = -13$ GHz, where $\Delta\nu = 1$ GHz is the Hopf bifurcation boundary. Between $\Delta\nu = -13$ GHz and $\Delta\nu = -22$ GHz is a region of locking–unlocking bistability, where the laser can be either locked or unlocked depending on the initial condition. Under that condition, the laser cannot be locked when the frequency detuning is more negative than -22 GHz. Relative to the free running laser, a broadband noise reduction occurs in the locked region when the injection field is negatively detuned beyond $\Delta\nu = -3$ GHz. The three representative values of frequency detuning chosen in this case are $\Delta\nu = 1$ GHz on the Hopf bifurcation boundary (dash-dotted curves in the figures), $\Delta\nu = -10$ GHz in the stable lock-

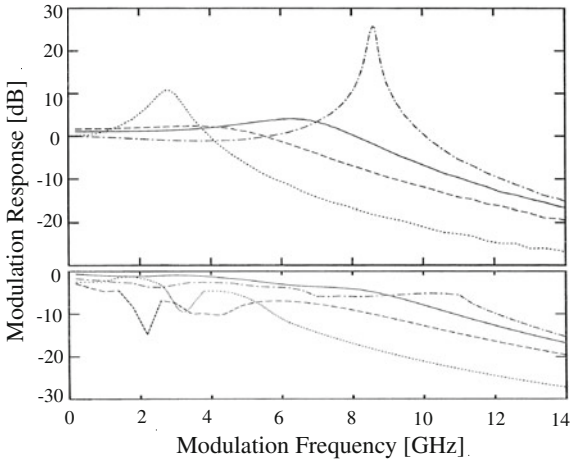

Fig. 6.12 Normalized current modulation response in the presence of frequency detuning $\Delta\nu$ between master and slave lasers. *Dash–dotted curve* injection locking at $\Delta\nu = 1$ GHz. *Solid curve* injection locking at $\Delta\nu = -10$ GHz. *Dashed curve*: injection locking at $\Delta\nu = -18$ GHz. *Dotted curve* free running. The *curves* in the *upper plot* are the response for m=1 %, and those in the *lower plot* are the responses for m=100 %. The 0 dB in the *lower plot* corresponds to the 0 dB in the *upper plot* in order to make all the response curves comparable [after Chen et al. (2000); © 2000 Elsevier]

ing region (solid curves), and $\Delta\nu = -18$ GHz in the locking-unlocking bistability region (dashed curves).

In the figure, the upper plot shows the response for a small modulation index of $m = 1\,\%$ and the graphs are normalized to the low frequency response of the laser in its free running condition, under the four different operating conditions. The lower plot in Fig. 6.12 shows the distorted current modulation response when the modulation index reaches $m = 100\,\%$. At a given modulation strength, negatively shifting the frequency detuning of the injected optical field generally reduces the distortion in the current modulation response if the laser remains stably locked. However, when the laser is injection-locked in the bistability region, a high modulation index can cause instability by unlocking the laser. As a result, the modulation response in such an operating condition becomes very irregular, as can be seen from the dashed curve (−18 GHz) in the lower plot of Fig. 6.12. For weak current modulation with small values of the modulation index, the modulation response will be obscured by the intrinsic laser noise. For the change of the modulation index, the laser noise induces insignificant differences between the overall response due to the combined modulation current and intrinsic noise and the modulation response alone when the modulation index m is larger than 1 %. Below $m = 1\,\%$, the relative importance of the laser noise gradually increases and the laser noise induces fluctuations in the response that obscure the modulation response.

Nevertheless optical feedback is strong, the optical injection power in the previous examples is still smaller than the solitary slave laser emission power. For stronger

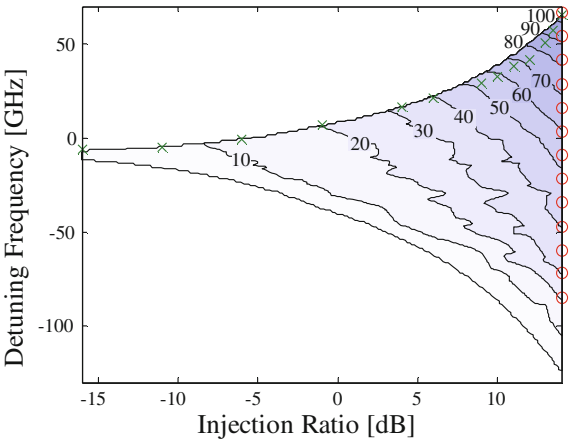

Fig. 6.13 Enhanced resonance frequency as a function of detuning frequency and injection ratio. Each value denotes the enhanced boundary resonance frequency [after Lau et al. (2008); © 2008 OSA]

optical injection above the slave optical power, we can expect much broader bandwidth enhancement. Figure 6.13 shows such an example. Lau et al. (2008) experimentally investigated modulation bandwidth for the condition of ultra strong optical injection more than +10 dB and large frequency detuning of about ±100 GHz. The figure shows the boundaries of enhanced resonance frequencies in the phase space of the optical injection ratio and the frequency detuning within the stable region of a used laser. The laser used is an InGaAsP DFB laser of the cavity length of 500 μm operating at a wavelength of 1.55 μm. The bias injection current is $1.3J_{\text{th}}$ and the corresponding relaxation oscillation frequency at solitary mode is $\nu_R = 3$ GHz. For an optical injection of 18 dB (the actual optical injection is estimated as about 14 dB due to losses in the optical system) and the frequency detuning from the solitary laser of +67 GHz, the modulation bandwidth is enhanced up to 107 GHz. By strong optical injection ratio with large frequency detuning, the stable area is largely expanded, especially in the region of strong optical injection. The attained value of the resonance frequency of 107 GHz is not the limitation of the device characteristic itself, but the result is limited only by the response of the equipment. Lau et al. also studied an enhancement of a modulation bandwidth for a VCSEL of a wavelength of 1.55 μm. The laser is biased at $3J_{\text{th}}$ with the corresponding relaxation frequency of 5 GHz. The resonance frequency enhancement of 104 GHz is obtained for the optical injection of 13.6 dB and the frequency detuning of +102 GHz.

One of merits of optical injection locking in semiconductor lasers is the increase of rf gain. However, there exists a tradeoff between the enhancement of modulation bandwidth and the increase of rf gain. For a fixed optical injection ratio, the rf gain of a small amplitude modulation for the bias injection current varies with detuning. For a large positive frequency detuning, one can obtain a sharp and high peak of the resonance frequency; however, the gain for the lower frequency component tends to be lower than that for a case of smaller frequency detuning. On the other hand, a high rf gain but a small peak of the resonance frequency is attained for an optical

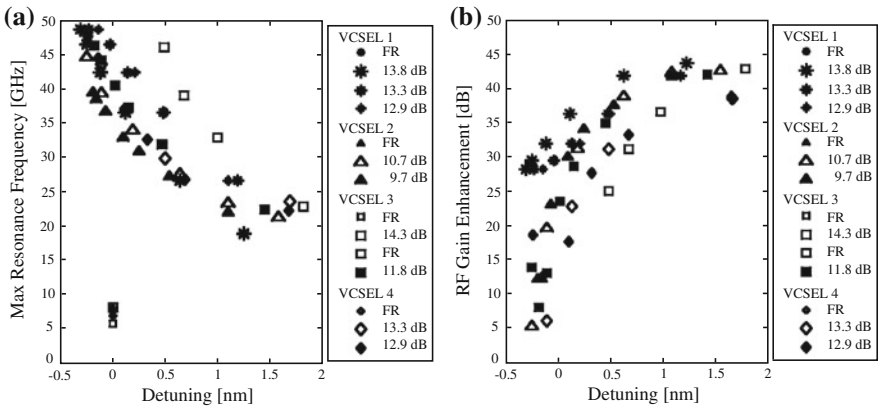

Fig. 6.14 Tradeoff between resonance frequency and rf gain. **a** Resonance frequency of four VCSELs versus wavelength detuning. **b** rf gain measured at 1 GHz for four VCSELs versus wavelength detuning [after Chrostowski et al. (2006); © 2006 IEEE]

injection with a small frequency detuning. Figure 6.14 shows a summary for such examples obtained by experiments (Chrostowski et al. 2006). Figure 6.14a is a plot for enhanced modulation frequencies for four VCSELs with almost the same optical injection ratios versus wavelength detuning. For the increase of the detuning, the modulation bandwidth is increased (it is noted that the graph is plotted not for the frequency but for the optical wavelength). While, Fig. 6.14b is a plot for enhanced resonance frequency at the injection–current modulation of 1 GHz versus wavelength detuning. With the increase of the frequency detuning, the rf gain decreases. The tradeoff is not a particular feature for VCSELs but other types of semiconductor lasers, and the similar trend can be expected for edge-emitting semiconductor lasers.

6.3.2 Origin of Modulation Bandwidth Enhancement

The origin of the enhancement of modulation bandwidth by strong optical injection is explained by Murakami et al. (2003). They consider the frequency shift of the slave laser induced by strong optical injection. The expansion of the modulation bandwidth is realized by the interference between the original optical frequency at the free running state and the shifted frequency after the injection. According to their explanation, the difference between the two frequencies corresponds to the expanded modulation bandwidth. Figure 6.15 schematically shows the model of the frequency shift. Let the angular frequency of the slave laser at the free running state be given by ω_0 and that of the master laser be ω_{inj}. In the figure, the frequency detuning is assumed to be positive, but the other case will be reduced to the same result. By a strong optical injection, the carrier density in the slave laser increases. This induces

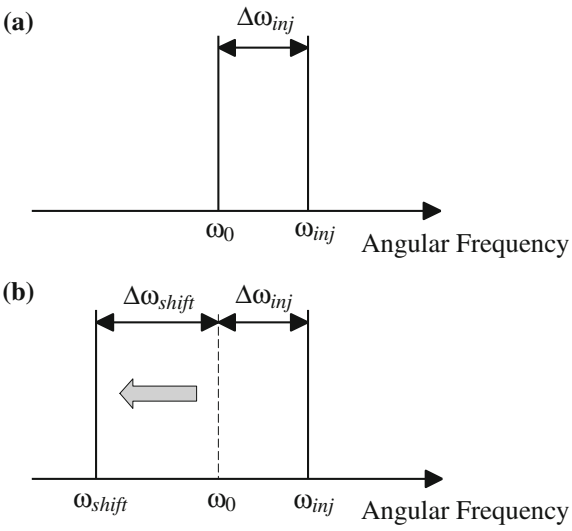

Fig. 6.15 Resonant condition of a semiconductor laser in the presence of optical injection. **a** Spectrum before optical injection. ω_0 is the angular frequency of the solitary laser, ω_{inj} is the frequency of the injected light, and $\Delta\omega_{\text{inj}}$ is the frequency detuning between them. **b** Cavity resonant condition under injection locking. ω_{shift} is the cavity resonance frequency shifted from ω_0 by $\Delta\omega_{\text{shift}}$ due to optical injection

the change of the optical frequency of the laser oscillation and results in red-shift of the oscillation frequency. Using the change of the carrier density δn, the laser once oscillates at an optical angular frequency ω_{shift} and the shift of the laser angular frequency after the injection is given by

$$\Delta\omega_{\text{shift}} = \frac{1}{2}\alpha G_n \delta n \tag{6.26}$$

The change of the carrier density δn is proportional to the strength of optical injection. The frequency shift given by (6.26) has the same form as the first term in (6.5). In actual fact, the frequency of the slave laser is locked to the frequency of the injection laser (angular frequency of ω_{inj}). Accordingly, the injection-locked laser may operate at a frequency different from its cavity resonance condition, namely operating at ω_{inj}, not at ω_{shift}. Such frequency detuning between ω_{inj} and ω_{shift} influences the modulation bandwidth, as predicted by Simpson et al. (1996).

Here, we consider the transient situation. The field corresponding to the shifted cavity resonance ω_{shift} is once excited and interference between the two components of the angular frequencies ω_{shift} and ω_{inj} occurs. Then, the beat between the two frequencies is induced in the output of the slave laser. However, sufficient gain is not allocated to this mode and the oscillation of the mode rapidly decays out, since this is a transient field. The oscillation angular frequency of the slave laser is restored to ω_{inj}. The laser output may exhibit a damping oscillation at the beat frequency due to such transient interference. Note that this damped oscillation differs from the relaxation oscillation in the physical mechanism, because the relaxation oscillation results from an interaction or coupling between photon and carrier through the stimulated emission. Therefore, from (6.5), the resonance angular frequency

produced by the interference $\omega_{\text{res}} = \omega_{\text{inj}} - \omega_{\text{shift}}$ is given by

$$\omega_{\text{res}} = \Delta\omega_{\text{inj}} - \Delta\omega_{\text{shift}} = -\frac{1}{\tau_{\text{in}}}\sqrt{\frac{S_{\text{inj}}}{S_s}}\sin\psi_s \tag{6.27}$$

Following the above explanation, the dependence of the resonance frequency in the presence of strong optical injection is calculated (Murakami et al. 2003). Figure 6.16 shows the plots of dependence of the injection ratio (amplitude) and the frequency detuning on the cutoff frequency. Figure 6.16a is the dependence of the cutoff frequency on the injection ratio at the frequency detuning of +0.5 GHz. Under a strong optical injection condition, the cutoff frequency is linearly proportional to the injection ratio in accordance with the prediction in (6.27). In the figure, three data are plotted; the solid line is the prediction calculated from (6.27), circles are the direct numerical calculation from the rate equations, and triangles are obtained from the linear stability analysis. In strong optical injection of over 30 %, the three plots coincide well with each other. Figure 6.16b is the plot of the cutoff frequency for the frequency detuning at a high optical injection ratio of 40 %. The cutoff frequency tends to increase with increased detuning from negative to positive values. Thus, the enhancement of the cutoff frequency under strong optical injection is explained by the interference between the injection laser frequency and the implicit frequency shift of the slave laser induced by the strong optical injection.

The definition of the injection and average intensities, S_{inj} and S_s, in (6.27) are the measures in the internal laser cavity. For the external injection intensity $S_{\text{inj,ext}}$, it has the relation with the internal intensity as Lau et al. (2007)

$$S_{\text{inj}} = \frac{(1-r_0^2)^2}{r_0^2}\frac{S_s}{S_{s,\text{out}}}S_{\text{inj,ext}} \tag{6.28}$$

where r_0 is the laser facet reflectivity defined in (4.1) and $S_{s,\text{out}}$ is the average intensity of the slave laser outside of the cavity. For edge-emitting semiconductor lasers, the orders of the magnitudes of internal and external injections are almost the same. In the case of VCSELs, the amount of the internally injected intensity is very small compared with that of the external intensity, since the facet reflectivity of VCSELs is usually higher than 99 %. On the other hand, the injection efficiency is proportional to $1/\tau_{\text{in}}$, so that the effect of optical injection to VCSELs is relatively strong due to their short cavity lengths. From (6.27), the attainable maximum enhanced modulation frequency is given by

$$\omega_{\text{res,max}} = \frac{1}{\tau_{\text{in}}}\sqrt{\frac{S_{\text{inj}}}{S_s}} \tag{6.29}$$

The above relation is well coincident with experimental results. From the detailed study, an approximate relation including a small resonance frequency, ω_{res}, due to weak optical injection is obtained as Lau et al. (2007, 2008, 2009)

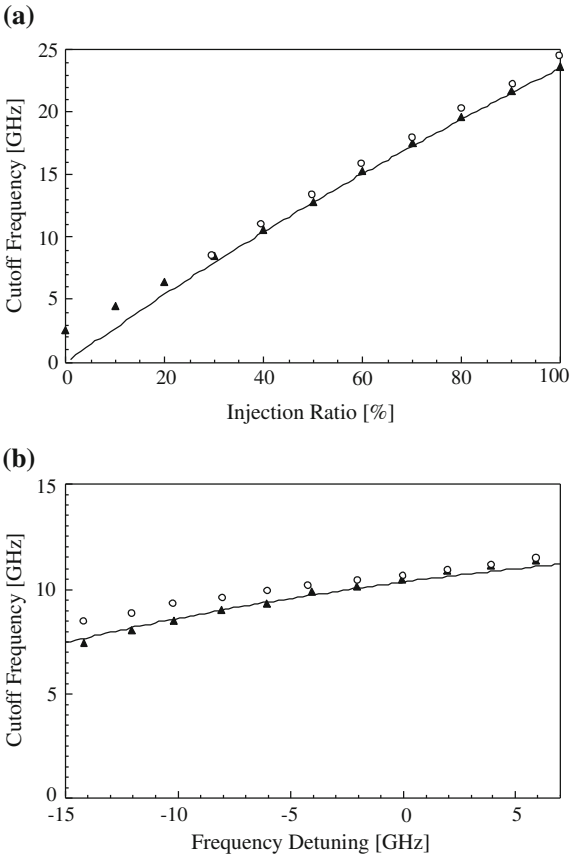

Fig. 6.16 Dependence of resonance frequency on **a** injection rate and **b** frequency detuning. *Circles* represent the numerical results, *triangles* are the results obtained from the stability analysis, and the *solid line* is the theoretical curve of (6.27)

$$\omega_{\text{enhanced}}^2 \approx \omega_R^2 + \omega_{\text{res}}^2 \tag{6.30}$$

where ω_R is the relaxation oscillation angular frequency of a solitary laser. For a large resonance frequency of $\omega_{\text{res}} \gg \omega_R$ (namely, strong optical injection), the relation $\omega_{\text{enhanced}} = \omega_{\text{res}}$ holds. In accordance with the enhancement of the modulation bandwidth, the damping factor is also enhanced. The damping factor except for near the resonance peak frequency under strong optical injection is approximated as

$$\Gamma_{\text{enhanced}} \approx \Gamma_R - G_n(n_{\text{th}} - n_0) \tag{6.31}$$

where Γ_R is the damping factor of the solitary laser defined in (3.70). Note that Γ_R is taken as a negative value. Also the damping factor is enhanced by the reduction of gain below threshold. The result is interpreted as follows; the injection-locked laser resonance is primarily due to energy oscillating between the slave field and phase interfering with the injected light from the master laser. The reduced gain allows a

portion of this oscillation energy to be lost to the carrier. We can observe the similarity of the damping enhancement in an RLC oscillator in electric circuits. On the other hand, the damping factor closed to the resonance frequency is given by

$$\Gamma_{\text{enhanced,res}} \approx \frac{\alpha}{\tau_{\text{ph}}\omega_{\text{res}}} G_n S_s - G_n(n_{\text{th}} - n_0) \tag{6.32}$$

Lau et al. (2009) also demonstrated theoretically and experimentally that the modulation bandwidth was further enhanced by amplitude and/or phase modulations of the master laser under strong optical injection.

6.3.3 Modulation Response by Strong Optical Injection

The effects of the injection current modulation on the response distortion and the noise compression can be evaluated by eye patterns with digital signals. The capability of data transmission in optical communications is calculated in Fig. 6.17 (Chen et al. 2000). The eye patterns are numerically calculated from the rate equations with strong optical injection. In the numerical simulations, eye patterns are generated by modulating the injection current of the semiconductor laser under the various operating conditions with a train of random raised-cosine functions:

$$J_m = \sum_{K=0}^{n} C_K h(t - KT) \tag{6.33}$$

$$h(t) = \frac{\sin\left(\frac{\pi t}{T}\right)\cos\left(\frac{\pi\beta_t t}{T}\right)}{\frac{\pi t}{T}\left[1 - \left(\frac{2\pi\beta_t t}{T}\right)^2\right]} \tag{6.34}$$

where C_K is a series of random numbers with the value 0 or 1, which represents digitized information, and $T = 1/f_m$, where the modulation frequency f_m represents the bit rate. The value of the parameter β_t is chosen to be 0.3 in this simulation.

Figure 6.17 shows the eye patterns for different modulation indexes at the modulation frequency of $f_m = 2.9$ GHz. The modulation frequency is equal to the relaxation oscillation frequency of the laser at the free running state. Three different modulation indexes $m = 10$, 50, and 100 % are chosen to present the advantages of the injection-locked laser in the stable locking region. The eye patterns obtained in the condition when the laser is injection-locked at $\Delta\nu = -10$ GHz have clearer eye opening with less distortion or less noise than those obtained in other operating conditions. The relative eye opening shows the same tendency as the noise compression. For a small modulation index of $m = 10$ %, the modulation efficiency is much improved compared with that at the free running state. However, when the modulation index

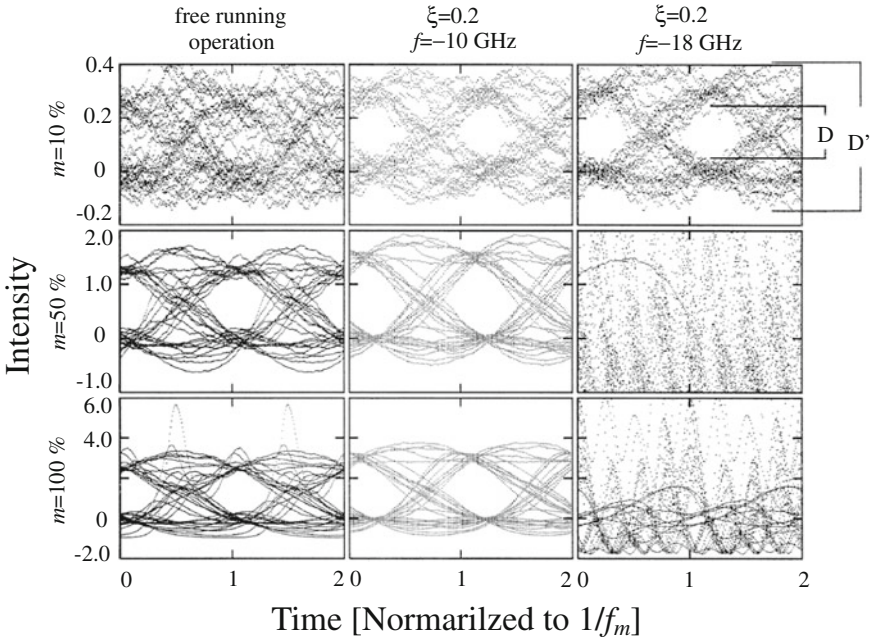

Fig. 6.17 Eye pattern for square wave modulations. The bit rate is chosen as the corresponding resonance frequency for each operating condition: the bit rate $f_m = 2.9$ GHz is chosen for the free running operation, $f_m = 4.7$ GHz for $\Delta\nu = -18$ GHz, and $f_m = 6.8$ GHz for $\Delta\nu = -10$ GHz. The optical injection rate ξ is defined as $\xi = \tau_{ph}\kappa_{inj}/\tau_{in}$. The eye opening obtained from the operating condition $\Delta\nu = 1$ GHz is zero for the range of the bit rate we are concerned with, so the eye patterns are not shown. The intensity of the eye patterns is the differential intensity above or below the corresponding field intensity of the injection-locked laser without current modulation for each operating condition [after Chen et al. (2000); © 2000 Elsevier]

increases, the modulation signal with a modulation index of $m = 50\,\%$ unlocks the laser for a large negative frequency detuning ($\Delta\nu = -18$ GHz), resulting in zero eye opening. When the frequency detuning is positively shifted beyond the noise compression region, the eye opening also rapidly decreases to zero. Therefore, the eye opening obtained in the operating condition with $\Delta\nu = 1$ GHz is zero for a modulation index of any value.

6.3.4 Suppression of Frequency Chirping by Strong Optical Injection

It has already been noted that the chirping of frequency due to injection current modulation in a semiconductor laser is much suppressed by a strong optical injection. We here demonstrate an example. Usually, a change in the carrier density causes a

change in the refractive index of the laser medium. This change in the index generates frequency chirping, which can place a considerable limitation on the modulation bit rate. The frequency chirping is measured by the normalized chirp to the power ratio CPR, which is defined as follows (Piazzolia et al. 1986):

$$\mathrm{CPR} = \frac{1}{2\pi R_P}\left|\frac{\mathrm{d}\phi}{\mathrm{d}t}\right| \tag{6.35}$$

where R_P is the modulation response. The frequency chirp originates from the linewidth enhancement factor α, which has a nonzero value in a semiconductor laser. Neglecting noise effects in a semiconductor laser and applying a small signal analysis, the relation between the linewidth enhancement factor α and CPR can be obtained by linearizing the rate equations around the locking operating point (Simpson et al. 1996). This relationship between α and the CPR can be expressed as follows:

$$\frac{1}{2\pi R_P}\left|\frac{\mathrm{d}\phi}{\mathrm{d}t}\right| \approx f_m\alpha\sqrt{\frac{f_m^2+(u-v/\alpha)^2}{f_m^2+(u+v/\alpha)^2}} \tag{6.36}$$

where u and v are given by

$$u = \frac{\kappa_{\mathrm{inj}}}{2\pi\tau_{\mathrm{in}}}\left|\frac{A_m}{A_s}\right|\cos\phi_L \tag{6.37}$$

$$v = \frac{\kappa_{\mathrm{inj}}}{2\pi\tau_{\mathrm{in}}}\left|\frac{A_m}{A_s}\right|\sin\phi_L \tag{6.38}$$

Here ϕ_L is the phase of the intracavity laser field relative to the injection field. An effective linewidth enhancement factor α_{eff}, which is the modified chirping parameter under injection locking, can be defined as follows:

$$\alpha_{\mathrm{eff}} \approx \alpha\sqrt{\frac{f_m^2+(u-v/\alpha)^2}{f_m^2+(u+v/\alpha)^2}} \tag{6.39}$$

Of course, the effective chirping parameter α_{eff} is equal to α when the laser is at the free running state ($u = v = 0$). The dependence of the effective chirping parameter on the modulation frequency f_m is shown in Fig. 6.18 (Chen et al. 2000). The injection locking of the laser at $\Delta\nu = -10$ GHz reduces the effective chirping parameter more than injection locking the laser at $\Delta\nu = -18$ GHz does. Positive shifting of the frequency detuning reduces the effective chirping parameter further until the boundary of the Hopf bifurcation is reached. For a large modulation index, the effective chirping parameter finally reaches that of the free running state. Therefore, the effect of the suppression for the chirping is remarkable for lower modulation frequency. When the effect of the intrinsic noise or that of the nonlinearity of the laser on the frequency chirping are significant, the simple relationship in (6.39) between the CPR

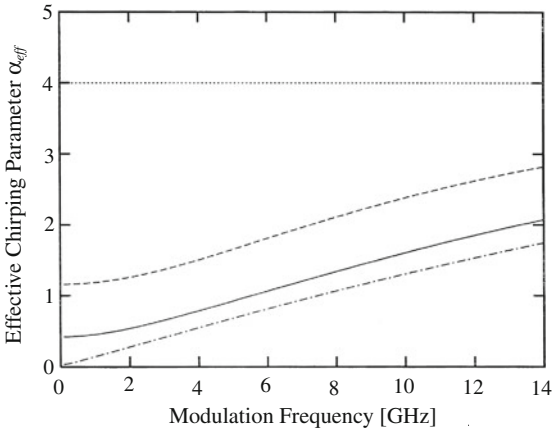

Fig. 6.18 Effective chirping parameter. Each *curve* corresponds directly to the curves in Fig. 6.12 that have the same style [after Chen et al. (2000); © 2000 Elsevier]

and α is no longer valid. In this situation, it is not possible to simply represent the frequency chirping with an effective chirping parameter. Then, the measurement of the frequency chirping including the effects of the intrinsic noise and the nonlinearity of the laser dynamics under a large modulation current is better quantified directly with the CPR.

From the detailed analysis for CPR, if the laser noise were not present, a significant reduction of the frequency chirping could be achieved by optical injection, and positively shifting the frequency detuning could further reduce the frequency chirping. In reality, however, when the modulation index is small, the chirp is dominated by the laser noise. As a result, the chirp follows the same tendency as the power noise. Therefore, reduction of the frequency chirping in a semiconductor laser is not always guaranteed by injection locking (Chen et al. 2000). A semiconductor laser injection-locked in a locking–unlocking bistable state cannot fully take such benefits because a large modulation current can unlock the laser. Further, one cannot operate in a state near or beyond the Hopf bifurcation boundary because of the high broadband noise and the large frequency chirping associated with the instability of the laser. A semiconductor laser operated in a stable state generally has better current modulation characteristics than in its free running state.

6.3.5 Generation of High-Frequency Chaotic Oscillation by Strong Optical Injection

Main chaotic carrier frequency in a semiconductor laser system has almost the same or nearly the relaxation oscillation frequency of the solitary laser. For example, the

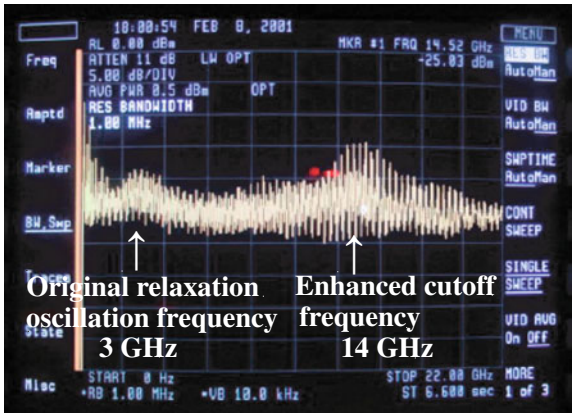

Fig. 6.19 Experimentally obtained chaotic power spectrum with enhanced cutoff frequency in a DFB semiconductor laser subjected to both optical feedback and strong optical injection. The frequency detuning between the two lasers is −3.44 GHz and the injection ratio is −5.61 dBm. The *left* and *right arrows* indicate the peaks for the chaotic carrier frequencies without and with optical injection, respectively

oscillation very close to the relaxation oscillation frequency is at first excited in a semiconductor laser with optical feedback for the increase of the feedback strength. For a further increase of the feedback, the laser typically shows chaotic oscillations via period-doubling or quasi-period-doubling routes. Therefore, the relaxation oscillation frequency of the laser is the measure of chaotic oscillations and it plays a crucial role in the chaotic dynamics. Especially, the bandwidth of the chaotic signal is important in the chaotic secure communications discussed in Chap. 13. In such chaotic communications, the generation of a fast chaotic carrier signal is essential for a message transmission with higher bit rate. We here consider the generation of fast chaotic signals in semiconductor lasers both subjected to optical feedback and optical injection. There are two ways for enhancing chaotic carrier frequency by optical injection; one is a simple method in which a chaotic semiconductor laser such as induced by optical feedback is strongly optical-injected by a stable master laser (Wang et al. 2008). The other one is that a chaotic master laser light is strongly injected to a slave laser (Someya et al. 2009). The slave laser may behave stably at solitary mode. For either case, chaotic carrier frequency of an original relaxation oscillation of about 3 GHz is experimentally expanded up to 15–20 GHz under appropriate optical injection conditions. In the preceding sections, we only treated the enhancement of the modulation bandwidth due to optical injection in stable region. However, outside of stable area in the phase space of the frequency detuning and the optical injection ratio, there exist regions of chaotic oscillations as is discussed in Fig. 6.6. Therefore, the discussion for chaotic carrier enhancement under optical injection is not straightforward. In the following, we treat the case of the bandwidth enhancement in chaotic semiconductor laser with optical feedback by strong optical injection from a stable laser. Therefore, we here restrict the discussion of chaotic carrier enhancement for stable region.

Figure 6.19 is a typical power spectrum of chaotic oscillations obtained from a semiconductor laser which has both external optical feedback and strong optical injection. Without a strong optical injection, the laser shows chaotic oscillation due

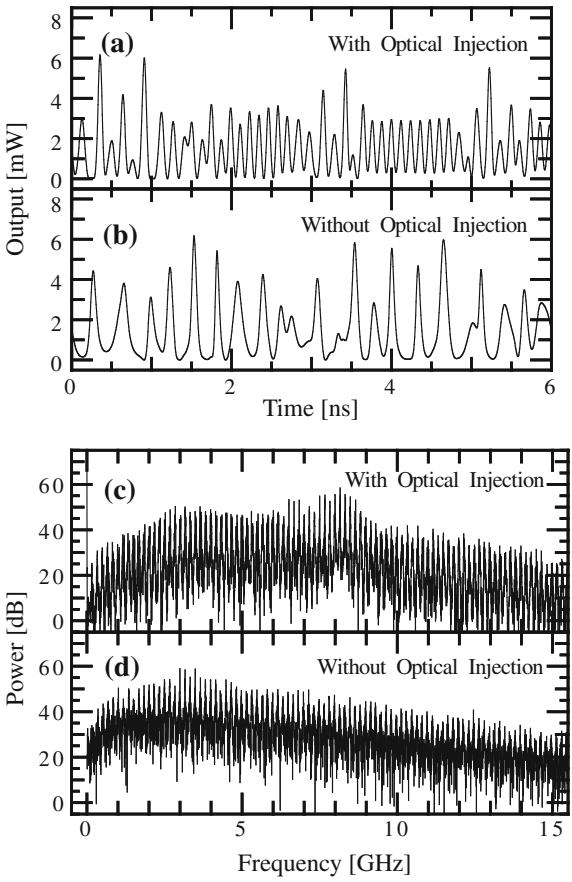

Fig. 6.20 Numerically calculated time series and power spectra of chaotic oscillations in a semiconductor laser with strong optical injection. Time series **a** with and **b** without optical injection. Power spectra **c** with and **d** without optical injection corresponding to Fig. 6.20a and b, respectively. The parameter conditions are $J_{s,m} = 1.3J_{\text{th}}$, $\tau = 6\,\text{ns}$, $\kappa/\tau_{\text{in}} = 2.33 \times 10^{10}\text{s}^{-1}$, $\kappa_{\text{inj}}/\tau_{\text{in}} = 1.79 \times 10^{10}\text{s}^{-1}$, and $\Delta\nu = -4\,\text{GHz}$

to the external optical feedback and the spectral peak (though it has a broad peak) is about 3 GHz, which is comparable with the relaxation oscillation of the solitary laser. The original relaxation oscillation frequency is shown by the arrow (left arrow). On the other hand, the frequency of the maximum chaotic oscillation is increased to 14 GHz (right arrow) by a strong optical injection, that is an increase by a factor of 4.6. In this experimental example, the frequency detuning between the master and slave lasers is −3.44 GHz and the optical injection ratio is −5.61 dBm. This condition corresponds to the ordinary stable operation in the absence of external optical feedback.

The enhancement of the chaotic carrier frequency is also numerically calculated based on the rate equations. Figure 6.20 is the result (Takiguchi et al. 2003). Figure 6.20a and b is the time series of chaotic oscillations with and without optical injection, respectively. The relaxation oscillation frequency of the solitary laser is about 2.7 GHz. Figure 6.20c and d is the corresponding rf spectra to Fig. 6.20a and b, respectively. The feedback fraction to the slave laser is taken to be a large

value of $\kappa/\tau_{in} = 2.33 \times 10^{10} s^{-1}$ to destabilize the strongly injection-locked laser. In Fig. 6.20d, the chaotic oscillation rapidly decays out over the relaxation oscillation frequency without optical injection. On the other hand, the spectrum in Fig. 6.20c shows a bandwidth-enhanced chaotic oscillation in the presence of a strong optical injection. As can easily be seen both from the time series and the spectrum, the chaotic carrier frequency is greatly expanded up to about 8 GHz by the strong optical injection, which is as much as three times that without optical injection in Fig. 6.20d. As shown in the figure, the chaotic carrier frequency is also greatly enhanced by a strong optical injection. However, it is difficult to calculate analytically the exact enhanced bandwidth of the chaotic carrier frequency.

References

Annovazzi-Lodi V, Donati S, Manna M (1994) Chaos and locking in a semiconductor laser due to external injection. IEEE J Quantum Electron 30:1537–1541

Chan SC, Liu JM (2004) Tunable narrow-linewidth photonic microwave generation using semiconductor laser dynamics. IEEE J Select Topics Quantum Electron 10:1025–1032

Chen HF, Liu JM, Simpson TB (2000) Response characteristics of direct current modulation on a bandwidth-enhanced semiconductor laser under strong injection locking. Opt Commun 173:349–355

Chrostowski L, Zhao X, Chang-Hasnain CJ (2006) Microwave performance of optically injection-locked VCSELs. IEEE Trans MTT 54:788–796

De Jagher PC, van der Graaf WA, Lenstra D (1996) Relaxation-oscillation phenomena in an injection-locked semiconductor laser. Quantum Semiclass Opt 8:805–822

Eriksson S, Lindberg AM (2001) Periodic oscillation within the chaotic region in a semiconductor laser subjected to external optical injection. Opt Lett 26:142–144

Erneux T, Kovanis V, Gavrielides A, Alsing PM (1996) Mechanism for period-doubling bifurcation in a semiconductor laser subject to optical injection. Phys Rev A 53:4372–4380

Furusawa A (1996) Amplitude squeezing of a semiconductor laser with light injection. Opt Lett 21:2014–2016

Gavrielides A, Kovanis V, Erneux T (1997) Analytical stability boundaries for a semiconductor laser subject to optical injection. Opt Commun 136:253–256

Genest J, Chamberland M, Tremblay P, Têtu M (1997) Microwave signals generated by optical heterodyne between injection-locked semiconductor lasers. IEEE J Quantum Electron 33:989–998

Heil T, Fischer I, Elsäßer W (1998) Coexistence of low-frequency fluctuations and stable emission on a single high-gain mode in semiconductor lasers with external optical feedback. Phys Rev A 58:R2672–R2675

Heil T, Fischer I, Elsäßer W (1999) Influence of amplitude-phase coupling on the dynamics of semiconductor lasers subject to optical feedback. Phys Rev A 60:634–641

Hwang SK, Liu JM (2000) Dynamical characteristics of an optically injected semiconductor laser. Opt Commun 183:195–205

Kovanis V, Gavrielides A, Simpson TB, Liu JM (1995) Instabilities and chaos in optically injected semiconductor lasers. Appl Phys Lett 67:2780–2782

Lau EK, Sung HK, Wu MC (2007) Scaling of resonance frequency for strong injection-locked lasers. Opt Lett 32:3373–3375

Lau EK, Zhao X, Sung HK, Parekh D, Chang-Hasnain CJ, Wu Ming CMC (2008) Strong optical injection-locked semiconductor lasers demonstrating >100-GHz resonance frequencies and 80-GHz intrinsic bandwidths. Opt Express 16:6609–6618

Lau EK, Wong LJ, Wu MC (2009) Enhanced modulation characteristics of optical injection-locked lasers: a tutorial. IEEE J Select Topics Quantum Electron 15:618–633
Lee EK, Pang HS, Park JD, Lee H (1993) Bistability and chaos in an injection-locked semiconductor laser. Phys Rev A 47:736–739
Lenstra D, van Tartwijk GHM, van der Graaf WA, De Jagher PC (1993) Multiwave-mixing dynamics in a diode laser. SPIE Proc 2039:11–22
Li L (1994a) Static and dynamic properties of injection-locked semiconductor lasers. IEEE J Quantum Electron 30:1701–1708
Li L (1994b) A unified description of semiconductor lasers with external light injection and its application to optical bistability. IEEE J Quantum Electron 30:1723–1731
Liu JM, Simpson TB (1994) Four-wave mixing and optical modulation in a semiconductor laser. IEEE J Quantum Electron 30:957–966
Liu JM, Chen HF, Tang S (2001) Optical-communication systems based on chaos in semiconductor lasers. IEEE Trans Circuits Syst I 48:1475–1483
Masoller C, Abraham NB (1998) Stability and dynamical properties of the coexisting attractors of an external-cavity semiconductor laser. Phys Rev A 57:1313–1322
Mogensen F, Olesen H, Jacobsen G (1985) Locking conditions and stability properties for a semiconductor laser with external light injection. IEEE J Quantum Electron 21:784–793
Murakami A, Kawashima K, Atsuki K (2003) Cavity resonance shift and bandwidth enhancement in semiconductor lasers with strong light injection. IEEE J Quantum Electron 39:1196–1194
Piazzolia S, Spano P, Tamburrini T (1986) Small signal analysis of frequency chirping in injection-locked semiconductor lasers. IEEE J Quantum Electron 22:2219–2223
Ryan A, Agrawal GP, Gray GR, Gage EC (1994) Optical feedback-induced chaos and its control in multimode semiconductor lasers. IEEE J Quantum Electron 30:668–679
Sacher J, Baums D, Panknin P, Elsäßer W, Göbel EO (1992) Intensity instabilities of semiconductor lasers under current modulation, external light injection, and delayed feedback. Phys Rev A 45:1893–1905
Schunk N, Petermann K (1986) Noise analysis of injection-locked semiconductor injection lasers. IEEE J Quantum Electron 22:642–650
Simpson TB (2003) Mapping the nonlinear dynamics of a distributed feedback semiconductor laser subjected to external optical injection. Opt Commun 215:135–151
Simpson TB, Liu JM (1997) Enhanced modulation bandwidth in injection-locked semiconductor lasers. IEEE Photon Technol Lett 9:1322–1324
Simpson TB, Liu JM, Gavrielides A (1995) Bandwidth enhancement and broadband noise reduction in injection-locked semiconductor lasers. IEEE Photon Technol Lett 7:709–911
Simpson TB, Liu JM, Gaverielides A (1996) Small-signal analysis of modulation characteristics in semiconductor laser subject to strong optical injection. IEEE J Quantum Electron 32:1456–1468
Simpson TB, Liu JM, Huang KF, Tai K (1997) Nonlinear dynamics induced by external optical injection in semiconductor lasers. Quantum Semiclass Opt 9:765–784
Simpson TB, Doft F, Strzelecka E, Liu JJ, Chang W, Simonis GJ (2001) Gain saturation and the linewidth enhancement factor in semiconductor lasers. IEEE Photon Technol Lett 13:776–778
Someya H, Oowada I, Okumura H, Kida T, Uchida A (2009) Synchronization of bandwidth-enhanced chaos in semiconductor lasers with optical feedback and injection. Opt Express 17:19536–19543
Sukow DW, Heil T, Fischer I, Gavrielides A, Hohl-AbiChedid A, Elsäßer W (1999) Picosecond intensity statistics of semiconductor lasers operating in the low-frequency fluctuation regime. Phys Rev A 60:667–673
Takiguchi Y, Ohyagi K, Ohtsubo J (2003) Bandwidth-enhanced chaos synchronization in strongly injection-locked semiconductor lasers with optical feedback. Opt Lett 28:319–321
van Tartwijk GHM, Agrawal GP (1998) Laser instabilities: a modern perspective. Prog Quantum Electron 22:43–122
Viktorov EA, Mandel P (2000) Low frequency fluctuations in a multimode semiconductor laser with optical feedback. Phys Rev Lett 85:3157–3160

Wang J, Haldar MK, Li L, Mendis VC (1996) Enhancement of modulation bandwidth of laser diodes by injection locking. IEEE Photon Technol Lett 8:34–36
Wang AB, Wang Y, He H (2008) Enhancing the bandwidth of the optical chaotic signal generated by a semiconductor laser with optical feedback. IEEE Photon Technol Lett 20:1633–1635
Wieczorek S, Krauskopf B, Lenstra D (2000) Mechanisms for multistability in a semiconductor laser with optical injection. Opt Commun 183:215–226
Wieczorek S, Krauskopf B, Lenstra D (2001a) Unnested islands of period doublings in an injected semiconductor laser. Phys Rev E 64:056204-1–9
Wieczorek S, Krauskopf B, Lenstra D (2001b) Sudden chaotic transitions in an optically injected semiconductor laser. Opt Lett 11:816–818
Wieczorek S, Krauskopf B, Lenstra D (2001c) Bifurcation transitions in an optically injected diode laser: theory and experiment. Opt Commun 215:125–134
Wieczorek S, Simpson TB, Krauskopf B, Lenstra D (2002) Global quantitative predictions of complex laser dynamics. Phys Rev E 65:R045207-1–4
Yabre G (1996) Effect of relatively strong light injection on the chirp-to-power ratio and the 3 dB bandwidth of directly modulated semiconductor lasers. J Lightwave Technol 14:2367–2373